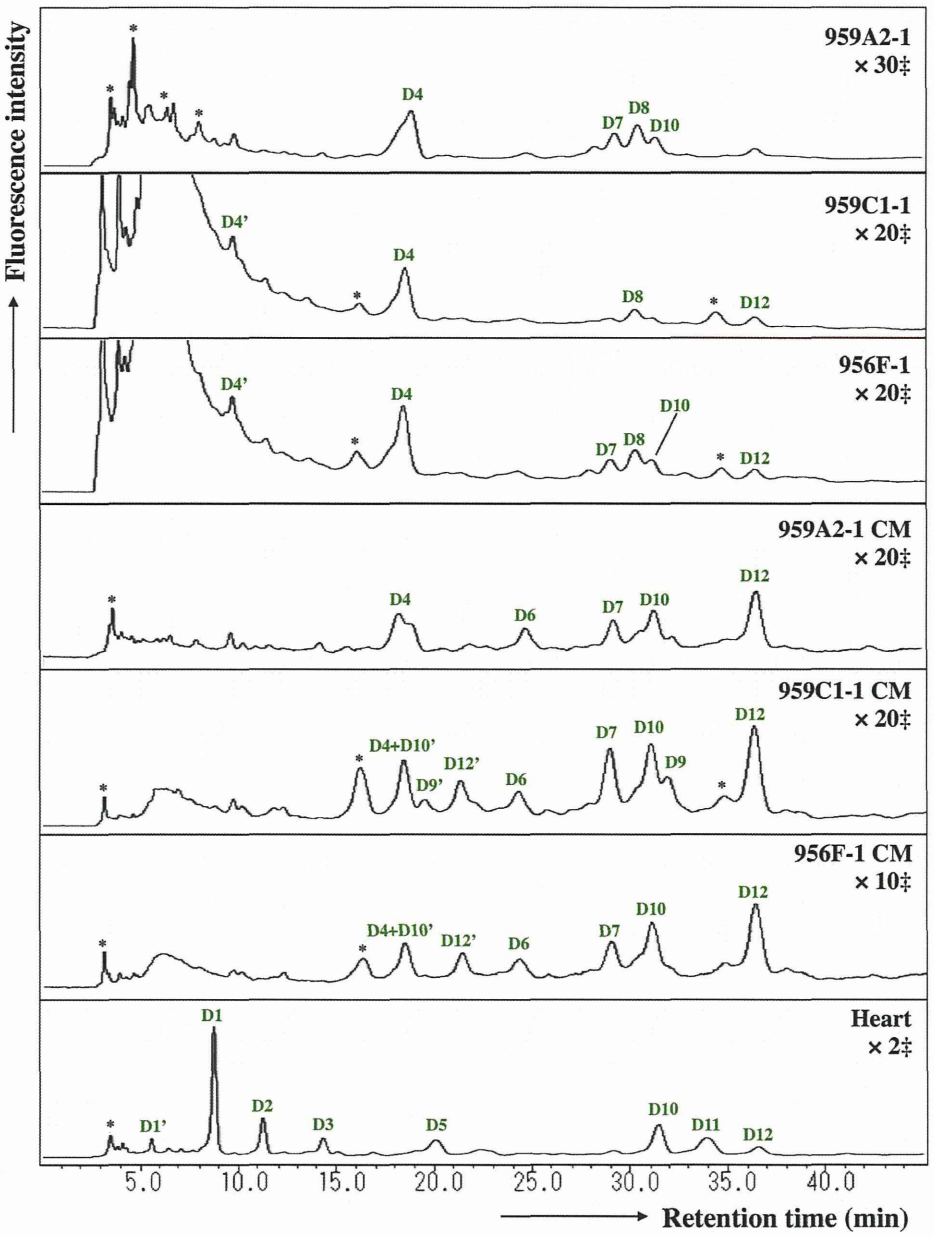

Figure 7. Reverse-phase ODS elution profiles of disialyl PA-glycans. The disialyl fractions were individually applied to the ODS column and eluted according to their hydrophobicity. D1′, D4′, D10′ and D12′: epimerization of D1, D4, D10 and D12; *Fractions containing no detectable PA-oligosaccharides. ‡Magnification ratio to the fluorescence intensity of asialoglycan of each sample.
doi:10.1371/journal.pone.0111064.g007

MS data. The coordinates of 54 *N*-glycans coincided with those for known references in the GALAXY database and their structures were identified. The coordinates for N9-3, M8, M11-2, M12, M13, M15, M17, M18, M19, M20-2, M21, M23, D8 and D9 did not correspond to known references.

N-glycans N9-2, M8, M12, M17, and M23 were trimmed by α-galactosidase but not by β-galactosidase or *N*-acetylglucosamidase. Their structures fit GALAXY references H5.12, 1A1-200.4, 1A3-200.4, 1A1-210.4, and 1A3-210.4, respectively. The galactosyl structures were then identified as Galα1-6Gal, because of the α-galactosidase-driven MS shifts. The structure of the M13 was identified by the coincidence with a GALAXY reference 1A2-H5.12 after being trimmed by α-L-fucosidase. The other *N*-glycans M11-2, M15, M18, M19, M20-2, M21, D8 and D9 were not identified in this study because they did not correspond to GALAXY references even after α-galactosidase digestions. They are described in Figure 8 and Table S1-S5 with their proposed formulas based on MALDI-TOF/MS data.

High-mannose *N*-Glycans were reduced by cardiomyogenic differentiation

The quantity of high-mannose *N*-glycans (HM) calculated from the total volume of N1–N6-2, N7 was highest in the iPSCs (959A2-1: 87.7%, 959C1-1: 68.3% and 956F-1: 78.2%), lower in the

Code No.	N1	N2-1	N2-2	N3	N4	N5	N6-1	N6-2	N6-3	N7	N8	N9-1
GU; ODS (Amid)	5.0 (8.8)	5.3 (7.9)	5.3 (9.5)	6.0 (7.8)	6.2 (7.0)	7.3 (6.0)	7.6 (4.2)	7.6 (5.0)	7.6 (4.6)	7.9 (3.3)	8.1 (7.3)	8.2 (5.6)
Mass (Da)	1800	1638	1962	1638	1475	1313	989	1151	1192	827	1679	1354
Structure	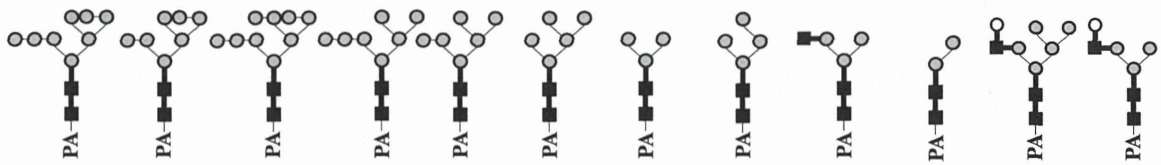											

N9-2	N9-3	N10	N11-1	N11-2	N11-3	N12	N13	N14	N15	N16	N17
8.2 (6.4)	8.3 (8.2)	9.3 (5.0)	10.5 (3.7)	10.5 (4.6)	10.5 (6.9)	11.2 (6.1)	12.8 (5.3)	13.0 (5.0)	13.3 (6.2)	13.5 (6.3)	14.2 (7.3)
1516	1841	1395	973	1135	1720	1500	1541	1338	1704	1704	1866
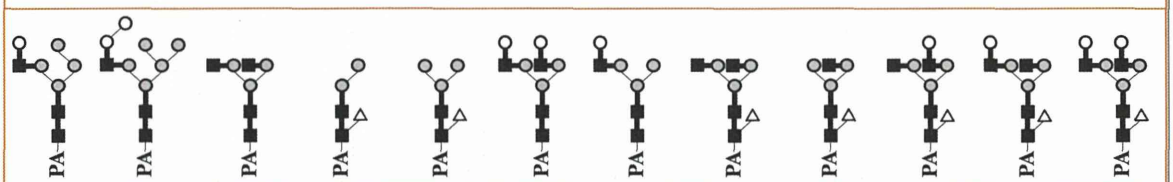											

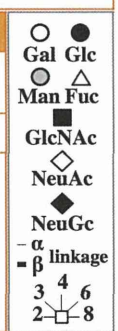

M1	M2-1	M2-2	M2-3	M3	M4	M5	M6-1	M6-2	M7	M8	M9	M10	M11-1	M11-2
7.6 (7.5)	7.9 (5.8)	7.9 (6.6)	7.9 (7.5)	8.1 (7.5)	8.4 (6.7)	8.6 (7.0)	9.0 (5.3)	9.0 (6.1)	10.1 (7.1)	10.3 (7.9)	10.6 (7.1)	11.0 (6.3)	11.3 (6.6)	11.3 (8.8)
1970	1646	1808	2027	1986	1824	1970	1646	1808	2011	2173	2027	1792	2011	2360
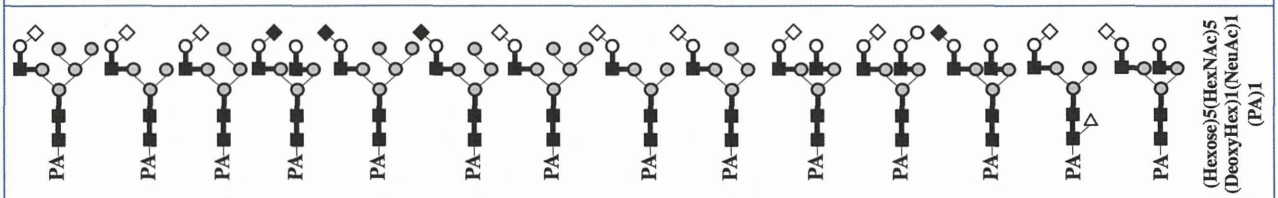														

M12	M13	M14-1	M14-2	M15	M16	M17	M18	M19	M20-1	M20-2	M21	M22	M23
11.5 (7.4)	11.3 (7.4)	11.8 (6.5)	11.8 (5.6)	12.1 (8.3)	13.3 (7.5)	13.7 (8.3)	13.8 (7.4)	14.0 (8.2)	14.2 (7.5)	14.2 (8.2)	14.5 (8.3)	15.1 (6.9)	15.3 (7.8)
2173	2116	1954	1792	2173	2157	2320	2360	2522	2173	2522	2344	2157	2320
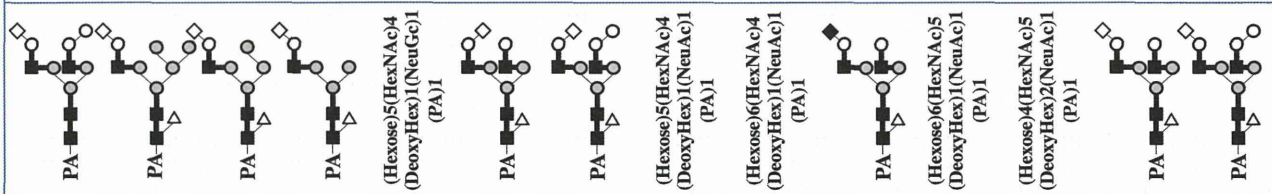													

D1	D2	D3	D4-1	D4-2	D5-1	D5-2	D6	D7	D8	D9	D10-1	D10-2	D11	D12
7.0 (8.2)	8.3 (7.8)	9.3 (8.6)	10.6 (6.9)	10.6 (7.3)	10.9 (7.4)	10.9 (8.1)	12.1 (6.4)	13.5 (7.7)	13.9 (6.8)	14.1 (7.5)	14.2 (7.2)	14.2 (7.7)	15.0 (7.2)	15.9 (6.7)
2334	2334	2480	2302	2302	2334	2480	2302	2448	2537	2854	2448	2480	2464	2448
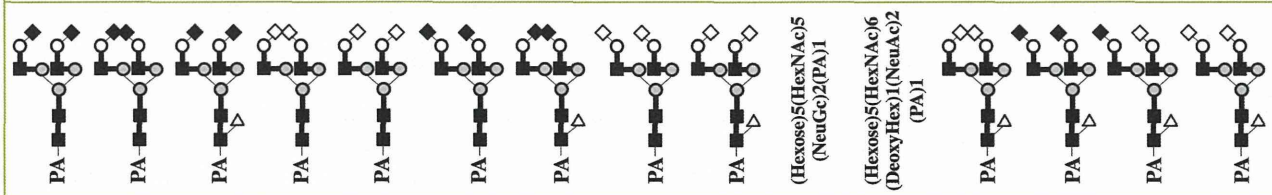														

Figure 8. Structures of neutral, monosialyl, and disialyl PA-oligosaccharides in iPSCs, iPSC-CM, and heart cells. Glucose units (GU) were calculated from the peak elution times for the ODS column in Figure 5, 6 and 7, and the amide column (data not shown). Average mass (Mass) calculated from the *m/z* values of $[M+Na]^+$ or $[M+H]^+$ ion for neutral, $[M-H]^-$ ion for monosialyl, and $[M-H]^-$ & $[M+Na-2H]^-$ ions for disialyl PA-oligosaccharides.
doi:10.1371/journal.pone.0111064.g008

iPSC-CMs (959A2-1 CM: 77.4%, 959C1-1 CM: 60.0% and 956F-1 CM: 65.1%), and lowest in the Heart (46.9%). The quantity of monofucosylated, difucosylated, and other types of *N*-glycans were greater in the iPSC-CMs and Heart (Figure 8, 9).

Sialyl *N*-glycans increased with cardiomyogenic differentiation

The quantity of monosialyl *N*-glycans (MS) calculated from the total volume of M1–M23 increased in iPSC-CMs (959A2-1 CM: 6.4%, 959C1-1 CM: 15.7% and 956F-1 CM: 10.5%) and Heart (19%) and were low in iPSCs (959A2-1: 0.5%, 959C1-1: 0.7% and 956F-1: 1.1%). The disialyl *N*-glycans (DS; D1–D12) yielded a similar pattern. The quantity of asialyl *N*-glycans (AS; N1–N17) decreased in iPSC-CMs (959A2-1 CM: 89.2%, 959C1-1 CM: 79.4% and 956F-1 CM: 81.7%) and Heart (55.3%) in comparison to the iPSCs (959A2-1: 96.9%, 959C1-1: 98.1% and 956F-1: 95.8%) (Figure 9, 10).

Rarely expressed *N*-glycans

The sialic acids identified in this study were either *N*-acetyl neuraminic acid (NeuAc) or *N*-glycolyl neuraminic acid (NeuGc). The quantity of monosialyl and disialyl *N*-glycans containing only NeuAc (A, A/A) was lowest in iPSCs (959A2-1: 2.5%, 959C1-1: 1.7% and 956F-1: 3.7%) and similar in iPSC-CMs (959A2-1 CM: 10.6%, 959C1-1 CM: 21% and 956F-1 CM: 18%) and the Heart (8%). The quantity of monosialyl and disialyl *N*-glycans containing only NeuGc (G, G/G) was markedly higher in the Heart (32.8%) than in iPSCs (959A2-1: 0.6%, 959C1-1: 0.1% and 956F-1: 0.5%) or iPSC-CMs (959A2-1 CM: 0%, 959C1-1 CM: 0% and 956F-1 CM: 0%) (Figure 10a).

Expression of glycosyl transferase, ST3Gal-III, ST3Gal-IV, ST6Gal-I, and CMAH in the iPSCs, iPSC-CMs, and Heart was assessed by RT-PCR to explore the glycan structures responsible for the differences between groups. The Heart expressed high levels of CMAH (0.91±0.13/GAPDH); levels in the iPSCs and iPSC-CMs were markedly lower (iPSCs: 959A2-1 0.011±0.0065/GAPDH, 959C1-1 0.013±0.0070/GAPDH, 956F-1 0.0045±0.0042/GAPDH, $P<0.05$; iPSC-CM: 959A2-1 CM 0.21±0.16/GAPDH, 959C1-1 CM 0.19±0.04, 956F-1 CM 0.45±0.31, $P<0.05$). Expression of ST3Gal-III was significantly higher in the Heart (0.98±0.13/GAPDH) than in iPSCs (959A2-1: 0.21±0.05/GAPDH, 959C1-1: 0.18±0.07/GAPDH, 956F-1: 0.27±0.05/GAPDH) and iPSC-CMs (959A2-1 CM: 0.40±0.10/GAPDH, 959C1-1 CM: 0.35±0.09/GAPDH, 956F-1 CM: 0.66±0.18); expression of ST3Gal-IV did not differ between groups. ST6Gal-I expression was significantly higher in iPSC-CMs (959A2-1 CM: 1.87±0.41/GAPDH, 959C1-1 CM: 1.95±0.22/GAPDH, 956F-1 CM: 3.08±1.27/GAPDH) than in iPSCs (959A2-1: 0.51±0.18/GAPDH, 959C1-1: 0.40±0.09/GAPDH, 956F-1: 0.62±0.29/GAPDH) and the Heart (1.04±0.13/GAPDH) (Figure 10b).

Discussion

Sixty-eight different *N*-glycans were isolated from iPSCs, iPSC-CMs, and the Heart. The structures of 60 *N*-glycans were identified, based on their HPLC elution peaks (Figure 8, Table S1-S5). Each preparation contained a combination of neutral, monosialyl, and disialyl *N*-glycans.

The molar ratios of high-mannose, monofucosylated, and difucosylated *N*-glycans were substantially different between groups (Figure 9), although no clear differences in the abundance of these glycans were found. The decrease in high-mannose *N*-glycans and increase of fucosylated *N*-glycans in iPSC-CMs versus iPSCs is consistent with a previous report on a comparison of ESC derived cardiomyocytes to undifferentiated ESCs [18]. Generally, all *N*-glycans are synthesized from the high-mannose type by a large array of sequentially and competitively acting biosynthetic enzymes located throughout the endoplasmic reticulum and Golgi apparatus [26], indicating that the high-mannose type of *N*-glycans could be categorized as a marker of immaturity. In this study, the high-mannose *N*-glycans were highest in the immature iPSC and lowest in the Heart, or mature tissue; thus, the quantity of high-mannose-type *N*-glycans might be an indicator of maturity in iPSC-derivatives and the iPSC-CMs in our protocol may still be immature in comparison to cardiac tissue.

Clear differences in glycan abundance were observed, such as hybrid and complex types represented by N9-1, N9-3, N15, N16, M1, M2-1, M2-2, M7, M8, M10, M12, M13, M14-1, M14-2, M17, M18, M20-2, D6 and D9 in iPSC-CMs, M2-3, M3, M4, M9, M11-1, M11-2, M20-1, M21, D1, D2, D3, D5-1, D5-2, D10-2 and D11 in Heart and N14 and M15 in iPSCs; these may also be indicators of maturation stage. In addition, expression of monosialyl and disialyl *N*-glycans in iPSC-CMs fell between the levels observed in the iPSCs and Heart, as were the molar ratios, indicating that the iPSC-CMs may still be immature stage. While many *N*-glycolyl neuraminic acid (NeuGc) structures were detected in the Heart, iPSCs and iPSC-CMs did not contain NeuGc in their sialyl structures, except for D8. Moreover, the molar ratio of NeuAc was low in iPSCs and iPSC-CMs. This finding is one of the clearest differences between iPSCs or iPSC-CMs and Heart cells.

The proposed spectra-based composition of the D8 glycans in iPSCs was [(Hexose)5(HexNAc)5(NeuGc)2(PA)1], indicating that it contains NeuGc. However, D8 might be quite a rare exception because transcript levels of CMAH, which catalyzes the conversion of NeuAc to NeuGc, was quite low in iPSCs in comparison to the Heart. This data suggests that during the process of reprograming, iPSCs suppress or eliminate CMAH activity. We conclude that iPSCs contain less sialic acid (especially NeuGc) and high-mannose structures are abundant in the *N*-glycans. In contrast, heart cells produce numerous sialyl-*N*-glycans, especially NeuGc. Transcript levels of CMAH tended to increase in iPSC-CMs relative to iPSCs, suggesting cardiomyogenic differentiation may induce expression of CMAH. If the iPSC-CMs could be matured more closely to the Heart by some additional methods of culture, the quantity of high mannose type of *N*-glycans might decrease more closely to the Heart, and might produce *N*-glycans containing NeuGc, followed by the expression of CMAH.

A terminal NeuGc, the Hanganutziu-Deicher (H-D) epitope [27], is widely distributed in the animal kingdom with the exception of humans and chickens. Expression of NeuGc is controlled by CMAH activity. Irie et al. [28] and Chou et al. [29] cloned the cDNA for human CMAH and reported that the *N*-terminal truncation of human CMAH is caused by deletion of Exon 6, a 92-base pair segment in the genomic DNA. Expression of this truncation in the heart eliminates NeuGc in sialyl

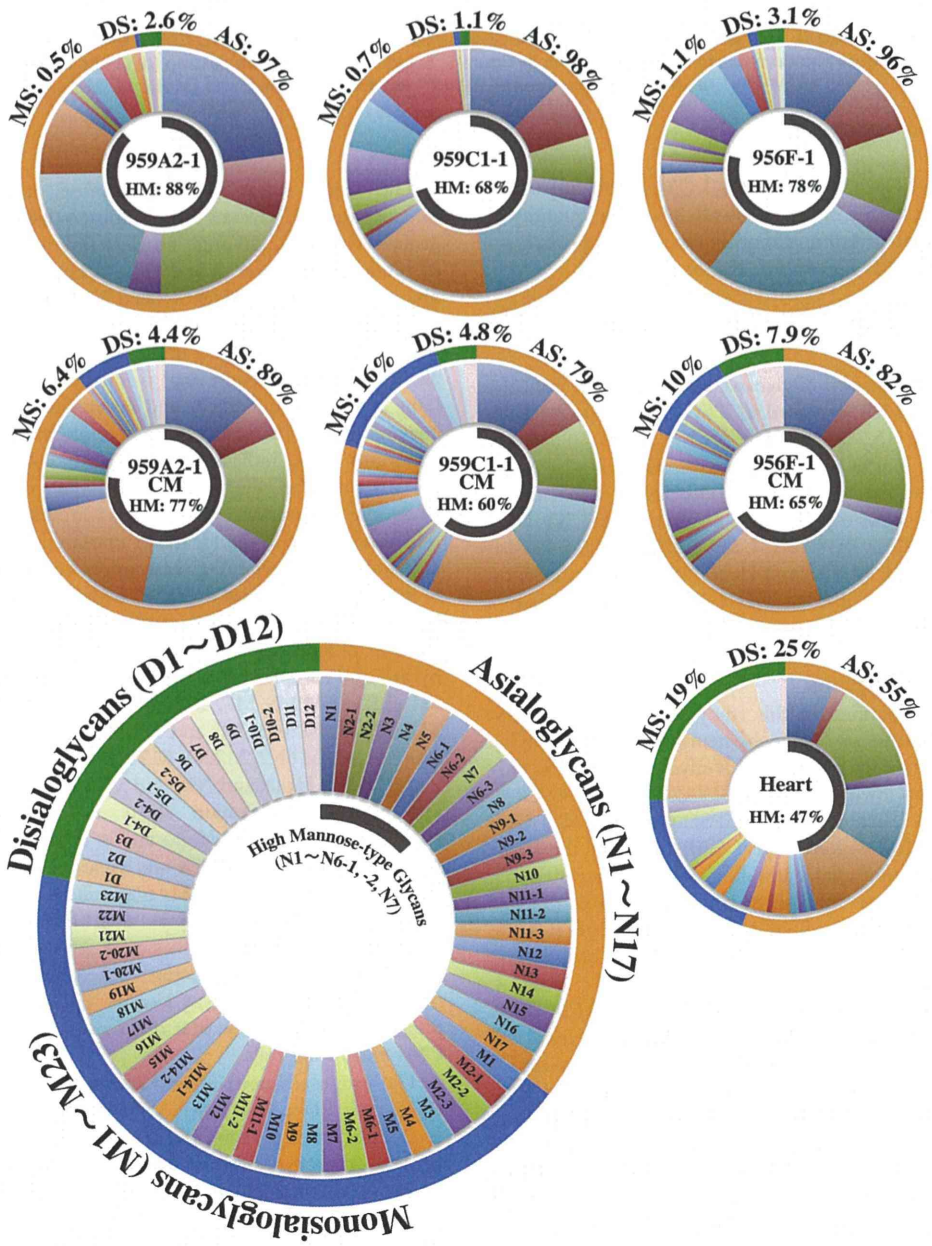

Figure 9. Relative quantities of neutral, monosialyl, and disialyl PA-oligosaccharides in iPSCs, iPSC-CM, and heart cells. Relative quantities of each glycan, calculated from the peak area in Figure 5, 6 and 7 vs. total *N*-glycan content in each cell, were expressed in the doughnut charts. Relative quantities of the asialoglycans, the monosialoglycans and the disialoglycans were showed outside of the charts, and relative quantities of the high mannose type glycans were showed inside of the charts. Asialoglycan (AS): the total volume of N1-N17; Monosialoglycan (MS): the total volume of M1-M23; Disialoglycan (DS): the total volume of D1-D12, High mannose-type glycan (HM): the total volume of N1–N6-1, N6-2, N7.
doi:10.1371/journal.pone.0111064.g009

structures. If human iPSCs or iPSC-CMs do not express CMAH in the same way as murine iPSCs or iPSC-CMs, there may be no difference between human iPSCs, iPSC-CMs, and the human Heart. Further study on human iPSC-CM will be needed to completely understand the features of the sialyl acid of *N*-glycans.

It was reported that human iPSCs produced α2,6sialyl glycans but did not contain α2,3sialyl structures, in contrast to human fibroblast, the origin of iPSCs, which produced α2,3sialyl but not α2,6sialyl structures [30,31]. The murine iPSCs in this study contained α2,3sialyl structures in NeuAc, M5, M23, D4-1, D10-1 and D12, and the iPSC-CMs produced α2,3 and α2,6sialyl structures in NeuAc. These differences may be due to variations between species, because mouse Heart cells also contained α2,3 and α2,6sialyl structures in NeuGc. Further studies are needed to characterize the glycome shift in the production and differentiation of iPSCs.

Type I Lactose structures were not detected, although over 98% of glycans in each cell were accounted for in this study. The *N*-glycans of N9-3, M8, M12, M17, and M23, which were identified after α-galactosidase digestion, contained Galα1-6Gal, not only in

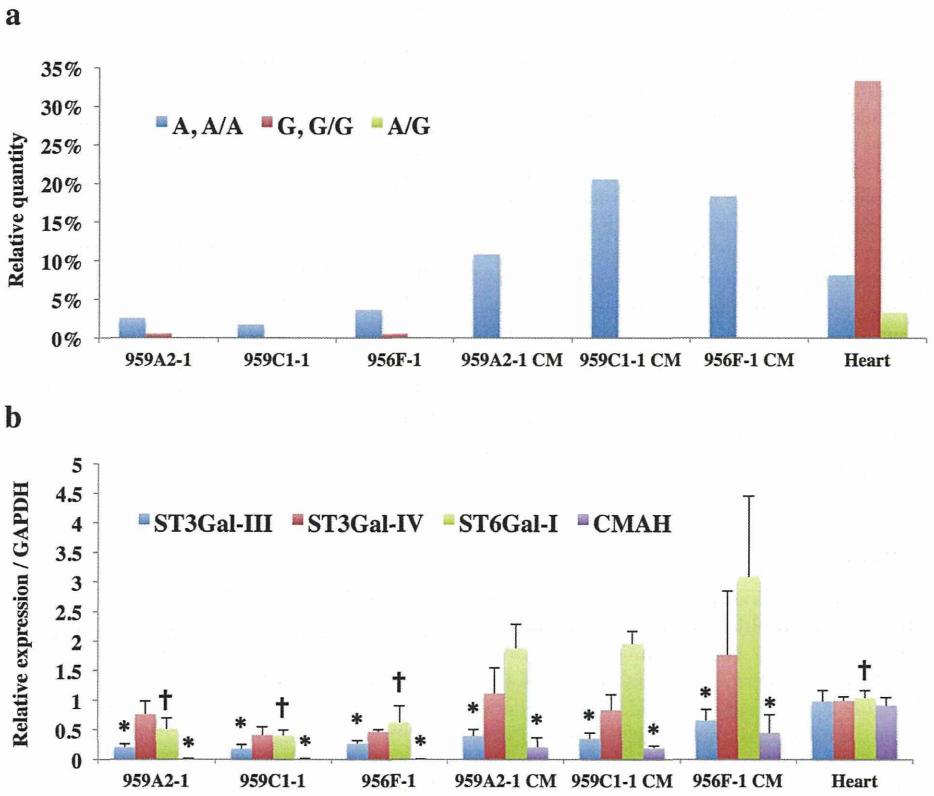

Figure 10. Rarely expressed NeuGc-containing glycans in iPSCs and iPSC-CMs. (a) Relative quantities of NeuAc- and NeuGc-containing glycans; Monosialoglycans containing NeuAc and Disialoglycans containing two NeuAc (A, A/A): the total volume of M1, M2-1, M2-2, M5-M8, M10-M14, M16-M19, M20-2, M21-M23, D4-1, D4-2, D6, D7, D9, D10-1, D12, Disialoglycan containing NeuAc and NeuGc (A/G): D11, Monosialoglycan containing NeuGc and Disialoglycan containing two NeuGc (G, G/G): the total volume of M2-3, M3, M4, M9, M15, M20-1, D1-D3, D5-1, D5-2, D8, D10-2. (b) Transcript expression of ST3Gal-III, ST3Gal-IV, ST6Gal-I, and CMAH; Transcript expression of glycosyltransferases in iPSCs, iPSC-CM, and heart cells was analyzed by real-time PCR. Results are expressed as the mean ± standard deviation. *P<0.05 vs. Heart, †P<0.05 vs. iPSC-CM (all of the 959A2-1 CM, 959C1-1 CM and 956F-1 CM).
doi:10.1371/journal.pone.0111064.g010

the neutral glycans but also in the monosialyl *N*-glycans of the iPSC-CM preparation. The same structure was not found in iPSCs, but only one structure, M23, was present in Heart cells. Therefore, in iPSC-CMs, Galα1-6Gal enzyme activity appears to be up-regulated in comparison to wild-type myocardium, although enzyme activity was not assessed by RT-PCR because of the limited availability of genetic sequence data.

The D8 was identified in all of three iPSC lines and not in the iPSC-CMs and Heart. This structure, unfortunately not identified in this study, may be useful as markers of undifferentiated iPSCs in the same way as well-known pluripotency biomarkers such as stage-specific embryonic antigens (SSEA)-3, SSEA-4 (glycosphingolipids) [32].

Previous MALDI-TOF/MS and MS/MS studies concluded that many kinds of *N*-glycans are found in organs and cells. The number of detected *N*-glycans is attributed to the sensitivity of the MS and HPLC methods employed. That is, MS data are sensitive and can be rapidly obtained, but a glycan structure is identified based only on the calculated molecular weight. Therefore, discriminating between isomeric structures is difficult. On the other hand, it thus appears that the accuracy of the data presented here using HPLC mapping in conjunction with a MALDI-TOF technique provides much more detailed information. Our data were used to identify the representative features of each *N*-glycan in these three cell types.

There may be a concern that the heart tissue used in this study contains connective tissues, vessels or nerves other than cardiomyocytes. Therefore, some of the *N*-glycans detected from the Heart sample might be derived from the tissues other than cardiomyocytes. However, heart is majority composed by cardiomyocytes, and furthermore, even if a small amount of *N*-glycans derived from connective tissues were contaminated in the Heart sample, the main evidences in this study, such as the proportion of the high-mannose type *N*-glycans, the ratio of the active sialyltransferase genes, the existence of NeuGc, and the uncommonness of Galα1-6 Gal, are essentially not affected.

In summary, murine iPSCs were rich in high-mannose type *N*-glycans but very poor in sialyl type *N*-glycans. Murine heart tissue contained a relatively low volume of high-mannose glycans, but was very rich in neuraminic acid, especially NeuGc type sialyl structures. Under these conditions, the volume of each type of glycan was similar for iPSC-CMs and iPSCs. That is, they were rich in high-mannose and relatively poor in sialyl type *N*-glycans by volume. In addition, most of the sialyl structures of the iPSC-CMs were different from those of the Heart, and the iPSC-CMs expressed no NeuGc. Moreover, the iPSC-CMs produced several unique glycans with the Galα1-6Gal structure. These results

provide important data that can be useful in future clinical iPSC studies.

It is quite important to investigate the meaning of *N*-glycans transitions during the cardiomyogenic differentiation presented in this study, for deeply understanding the relationship between the *N*-glycan expression and cardiomyogenic differentiation. Knock-out or knock-down of the genes related to cardiomyogenic differentiation or glycosylation may be useful for such purpose. However, the *N*-glycan signature in the cell surface is determined by a variety of the genes. Knock-out or knock-down of a single gene related to cardiomyogenic differentiation would alter an array of gene expressions, such as sarcomere proteins, transcriptional factors, or cell surface proteins, all of which would affect the signature of *N*-glycans in the cell surface. Therefore, the data interpretation for relationship between expression of a single gene and *N*-glycan signature would be difficult. Some different experimental approach may be needed to investigate the meaning of change in *N*-glycan expression during cardiomyogenic differentiation.

Supporting Information

Table S1 Structures and relative quantities of neutral (Table S1, S2) PA-oligosaccharides derived from iPSC, iPSC-CM, and heart cells. a. Glucose units (GU) were calculated from the peak elution times of the peaks obtained from the ODS column in Figure 5, 6, 7 and the Amide column (data not shown). b. Average mass calculated from the *mlz* values of $[M+Na]^+$ or $[M+H]^+$ ion for neutral, $[M-H]^-$ ion for mono-sialyl, and $[M-H]^-$ & $[M+Na-2H]^-$ ions for di-sialyl PA-oligosaccharides. c. PA-oligosaccharide structures. d. mol% was calculated from the peak area versus total *N*-glycan content in each cell
(TIFF)

Table S2 Structures and relative quantities of neutral (Table S1, S2) PA-oligosaccharides derived from iPSC, iPSC-CM, and heart cells.
(TIFF)

Table S3 Structures and relative quantities of mono-sialyl (Table S3, S4) PA-oligosaccharides derived from iPSC, iPSC-CM, and heart cells.
(TIFF)

Table S4 Structures and relative quantities of mono-sialyl (Table S3, S4) PA-oligosaccharides derived from iPSC, iPSC-CM, and heart cells.
(TIFF)

Table S5 Structures and relative quantities of disialyl PA-oligosaccharides derived from iPSC, iPSC-CM, and heart cells.
(TIFF)

Video S1
(MP4)

Acknowledgments

Our deepest appreciation goes to Professor Shinya Yamanaka and Keisuke Okita of the Center for iPS Cell Research and Application, Kyoto University, who kindly provided the murine iPSCs. We also thank Sachiko Kondo and Uichiro Yabe of MBL, Nagoya, Japan, who gave invaluable comments regarding *N*-glycan analysis.

Author Contributions

Conceived and designed the experiments: TK S. Miyagawa S. Miyagawa JL YS. Performed the experiments: TK AY NK AK EI AM HE KT. Analyzed the data: TK S. Miyagawa YS. Contributed reagents/materials/analysis tools: TK AY JL. Wrote the paper: TK S. Miyagawa YS SF. Obtained permission for use of cell line: S. Miyagawa AS YS.

References

1. Gonzales C, Pedrazzini T (2009) Progenitor cell therapy for heart disease. Exp Cell Res 315: 3077–3085.
2. Shah AM, Mann DL (2011) In search of new therapeutic targets and strategies for heart failure: recent advances in basic science. Lancet 378: 704–712.
3. Yoshida Y, Yamanaka S (2010) Recent stem cell advances: induced pluripotent stem cells for disease modeling and stem cell-based regeneration. Circulation 122: 80–87.
4. Yoshida Y, Yamanaka S (2011) iPS cells: A source of cardiac regeneration. Journal of Molecular and Cellular Cardiology 50: 327–332.
5. Kawamura M, Miyagawa S, Miki K, Saito A, Fukushima S, et al. (2012) Feasibility, safety, and therapeutic efficacy of human induced pluripotent stem cell-derived cardiomyocyte sheets in a porcine ischemic cardiomyopathy model. Circulation 126: S29–37.
6. Mercola M, Colas A, Willems E (2013) Induced pluripotent stem cells in cardiovascular drug discovery. Circ Res 112: 534–548.
7. Sinnecker D, Goedel A, Laugwitz KL, Moretti A (2013) Induced pluripotent stem cell-derived cardiomyocytes: a versatile tool for arrhythmia research. Circ Res 112: 961–968.
8. Kamakura T, Makiyama T, Sasaki K, Yoshida Y, Wuriyanghai Y, et al. (2013) Ultrastructural maturation of human-induced pluripotent stem cell-derived cardiomyocytes in a long-term culture. Circ J 77: 1307–1314.
9. Kuzmenkin A, Liang H, Xu G, Pfannkuche K, Eichhorn H, et al. (2009) Functional characterization of cardiomyocytes derived from murine induced pluripotent stem cells in vitro. FASEB J 23: 4168–4180.
10. Varki A (1993) Biological roles of oligosaccharides: all of the theories are correct. Glycobiology 3: 97–130.
11. Haltiwanger RS, Lowe JB (2004) Role of glycosylation in development. Annu Rev Biochem 73: 491–537.
12. Ohtsubo K, Marth JD (2006) Glycosylation in cellular mechanisms of health and disease. Cell 126: 855–867.
13. Surani MA (1979) Glycoprotein synthesis and inhibition of glycosylation by tunicamycin in preimplantation mouse embryos: compaction and trophoblast adhesion. Cell 18: 217–227.
14. Akama TO, Nakagawa H, Sugihara K, Narisawa S, Ohyama C, et al. (2002) Germ cell survival through carbohydrate-mediated interaction with Sertoli cells. Science 295: 124–127.
15. Hato M, Nakagawa H, Kurogochi M, Akama TO, Marth JD, et al. (2006) Unusual N-glycan structures in alpha-mannosidase II/IIx double null embryos identified by a systematic glycomics approach based on two-dimensional LC mapping and matrix-dependent selective fragmentation method in MALDI-TOF/TOF mass spectrometry. Mol Cell Proteomics 5: 2146–2157.
16. Lau KS, Partridge EA, Grigorian A, Silvescu CI, Reinhold VN, et al. (2007) Complex N-glycan number and degree of branching cooperate to regulate cell proliferation and differentiation. Cell 129: 123–134.
17. Kraushaar DC, Rai S, Condac E, Nairn A, Zhang S, et al. (2012) Heparan sulfate facilitates FGF and BMP signaling to drive mesoderm differentiation of mouse embryonic stem cells. J Biol Chem 287: 22691–22700.
18. Amano M, Yamaguchi M, Takegawa Y, Yamashita T, Terashima M, et al. (2010) Threshold in stage-specific embryonic glycotypes uncovered by a full portrait of dynamic N-glycan expression during cell differentiation. Mol Cell Proteomics 9: 523–537.
19. Okita K, Nakagawa M, Hyenjong H, Ichisaka T, Yamanaka S (2008) Generation of mouse induced pluripotent stem cells without viral vectors. Science 322: 949–953.
20. Miki K, Uenaka H, Saito A, Miyagawa S, Sakaguchi T, et al. (2012) Bioengineered myocardium derived from induced pluripotent stem cells improves cardiac function and attenuates cardiac remodeling following chronic myocardial infarction in rats. Stem Cells Transl Med 1: 430–437.
21. Yu T, Miyagawa S, Miki K, Saito A, Fukushima S, et al. (2013) In vivo differentiation of induced pluripotent stem cell-derived cardiomyocytes. Circ J 77: 1297–1306.
22. Tohyama S, Hattori F, Sano M, Hishiki T, Nagahata Y, et al. (2013) Distinct metabolic flow enables large-scale purification of mouse and human pluripotent stem cell-derived cardiomyocytes. Cell Stem Cell 12: 127–137.
23. Takahashi N, Khoo KH, Suzuki N, Johnson JR, Lee YC (2001) N-glycan structures from the major glycoproteins of pigeon egg white: predominance of terminal Galalpha(1)Gal. J Biol Chem 276: 23230–23239.

24. Takahashi N, Kato K (2003) GALAXY(Glycoanalysis by the Three Axes of MS and Chromatography): a Web Application that Assists Structural Analyses of N-Glycans. Trends in Glycoscience and Glycotechnology 15 No.84: 235–251.
25. Yagi H, Takahashi N, Yamaguchi Y, Kimura N, Uchimura K, et al. (2005) Development of structural analysis of sulfated N-glycans by multidimensional high performance liquid chromatography mapping methods. Glycobiology 15: 1051–1060.
26. Dalziel M, Crispin M, Scanlan CN, Zitzmann N, Dwek RA (2014) Emerging principles for the therapeutic exploitation of glycosylation. Science 343: 1235681.
27. Varki A (2009) Multiple changes in sialic acid biology during human evolution. Glycoconj J 26: 231–245.
28. Irie A, Koyama S, Kozutsumi Y, Kawasaki T, Suzuki A (1998) The molecular basis for the absence of N-glycolylneuraminic acid in humans. J Biol Chem 273: 15866–15871.
29. Chou HH, Takematsu H, Diaz S, Iber J, Nickerson E, et al. (1998) A mutation in human CMP-sialic acid hydroxylase occurred after the Homo-Pan divergence. Proc Natl Acad Sci U S A 95: 11751–11756.
30. Hasehira K, Tateno H, Onuma Y, Ito Y, Asashima M, et al. (2012) Structural and quantitative evidence for dynamic glycome shift on production of induced pluripotent stem cells. Mol Cell Proteomics 11: 1913–1923.
31. Tateno H, Toyota M, Saito S, Onuma Y, Ito Y, et al. (2011) Glycome diagnosis of human induced pluripotent stem cells using lectin microarray. J Biol Chem 286: 20345–20353.
32. Fujitani N, Furukawa J, Araki K, Fujioka T, Takegawa Y, et al. (2013) Total cellular glycomics allows characterizing cells and streamlining the discovery process for cellular biomarkers. Proc Natl Acad Sci U S A 110: 2105–2110.

Tissue Engineering Part A

Addition of Mesenchymal Stem Cells Enhances the Therapeutic Effects of Skeletal Myoblast Cell-Sheet Transplantation in a Rat Ischemic Cardiomyopathy Model

Yasuhiro Shudo, MD,[1] Shigeru Miyagawa, MD, PhD,[1] Hanayuki Ohkura, PhD,[1,2] Satsuki Fukushima, MD, PhD,[1] Atsuhiro Saito, PhD,[1] Motoko Shiozaki, PhD,[1] Naomasa Kawaguchi, PhD,[3] Nariaki Matsuura, MD, PhD,[3] Tatsuya Shimizu, MD, PhD,[4] Teruo Okano, PhD,[4] Akifumi Matsuyama, MD, PhD,[2] and Yoshiki Sawa, MD, PhD[1]

[1]Department of Cardiovascular Surgery, Osaka University Graduate School of Medicine, Suita, Japan.
[2]Laboratory for Somatic Stem Cell Therapy, Foundation of Biomedical Research and Innovation, Kobe, Japan.
[3]Department of Pathology, Osaka University Graduate School of Medicine, Suita, Japan.
[4]Institute of Advanced Biomedical Engineering and Science, Tokyo Women's Medical University, Tokyo, Japan.

Address correspondence to:
Yoshiki Sawa, MD, PhD
Department of Cardiovascular Surgery
Osaka University Graduate School of Medicine
Suita
Osaka 565-0871
Japan
E-mail: sawa-p@surg1.med.osaka-u.ac.jp

Received: September 2, 2012
Accepted: September 25, 2013

ABSTRACT

Introduction: Functional skeletal myoblasts (SMBs) are transplanted into the heart effectively and safely as cell sheets, which induce functional recovery in myocardial infarction (MI) patients without lethal arrhythmia. However, their therapeutic effect is limited by ischemia. Mesenchymal stem cells (MSCs) have prosurvival/proliferation and antiapoptotic effects on co-cultured cells *in vitro*. We hypothesized that adding MSCs to the SMB cell sheets might enhance SMB survival post-transplantation and improve their therapeutic effects.

Methods and Results: Cell sheets of primary SMBs of male Lewis rats (r-SMBs), primary MSCs of human female fat tissues (h-MSCs), and their co-cultures were generated using temperature-responsive dishes. The levels of candidate paracrine factors, rat hepatocyte growth factor and vascular endothelial growth factor, *in vitro* were significantly greater in the h-MSC/r-SMB co-cultures than in those containing r-SMBs only, by real-time PCR and enzyme-linked immunosorbent assay (ELISA). MI was generated by left-coronary artery occlusion in female athymic nude rats. Two weeks later, co-cultured r-SMB or h-MSC cell sheets were implanted or no treatment was performed (n=10 each). Eight weeks later, systolic and diastolic function parameters were improved in all three treatment groups compared to no treatment, with the greatest improvement in the co-cultured cell sheet transplantation group. Consistent results were found for capillary density, collagen accumulation, myocyte hypertrophy, Akt-signaling, STAT3 signaling, and survival of transplanted cells of rat origin, and were related to poly (ADP-ribose) polymerase-dependent signal transduction.

Conclusions: Adding MSCs to SMB cell sheets enhanced the sheets' angiogenesis-related paracrine mechanics and, consequently, functional recovery in a rat MI model, suggesting a possible strategy for clinical applications.

Cell Transplantation, Vol. 23, pp. 1305–1319, 2014

0963-6897/14 $90.00 + .00
DOI: http://dx.doi.org/10.3727/096368913X665602
E-ISSN 1555-3892
www.cognizantcommunication.com

Improvement of Cardiac Stem Cell Sheet Therapy for Chronic Ischemic Injury by Adding Endothelial Progenitor Cell Transplantation: Analysis of Layer-Specific Regional Cardiac Function

Sokichi Kamata,* Shigeru Miyagawa,* Satsuki Fukushima,* Satoshi Nakatani,†
Atsuhiko Kawamoto,‡ Atsuhiro Saito,* Akima Harada,* Tatsuya Shimizu,§
Takashi Daimon,¶ Teruo Okano,§ Takayuki Asahara,‡ and Yoshiki Sawa*

*Department of Cardiovascular Surgery, Osaka University Graduate School of Medicine, Suita, Japan
†Division of Functional Diagnostics, Department of Cardiovascular Medicine,
Osaka University Graduate School of Medicine, Suita, Japan
‡Division of Vascular Regeneration Therapy, Institute of Biomedical Research and Innovation, Kobe, Japan
§Institute of Advanced Biomedical Engineering and Science, Tokyo Women's Medical University, Tokyo, Japan
¶Department of Biostatistics, Hyogo College of Medicine, Nishinomiya, Hyogo, Japan

The transplantation of cardiac stem cell sheets (CSC sheets) is a promising therapeutic strategy for ischemic cardiomyopathy, although potential ischemia in the transplanted area remains a problem. Injected endothelial progenitor cells (EPCs) can reportedly induce angiogenesis in the injected area. We hypothesized that concomitant CSC sheet transplantation and EPC injection might show better therapeutic effects for chronic ischemic injury model than the transplantation of CSC sheets alone. Scaffold-free CSC sheets were generated from human c-kit-positive heart-derived cells. A porcine chronic ischemic injury model was generated by placing an ameroid constrictor around the left coronary artery for 4 weeks. The animals then underwent a sham operation, epicardial transplantation of CSC sheet over the ischemic area, intramyocardial injection of EPCs into the ischemic and peri-ischemic area, or CSC sheet transplantation plus EPC injection. The efficacy of each treatment was then assessed for 2 months. Speckle-tracking echocardiography was used to dissect the layer-specific regional systolic function by measuring the radial strain (RS). The epicardial RS in the ischemic area was similarly greater after treatment with the CSC-derived cell sheets alone (19±5%) or in combination with EPC injection (20±5%) compared with the EPC only (9±4%) or sham (7±1%) treatment. The endocardial RS in the ischemic area was greatest after the combined treatment (14±1%), followed by EPC only (12±1%), compared to the CSC only (11±1%) and sham (9±1%) treatments. Consistently, either epicardial CSC sheet implantation or intramyocardial EPC injection yielded increased capillary number and reduced cardiac fibrosis in the ischemic epicardium or endocardium, respectively. Concomitant EPC injection induced the migration of transplanted CSCs into the host myocardium, leading to further neovascularization and reduced fibrosis in the ischemic endocardium, compared to the CSC sole therapy. Transplantation of CSC sheets induced significant functional recovery of the ischemic epicardium, and concomitant EPC transplantation elicited transmural improvement in chronic ischemic injury.

Key words: Cardiac stem cells (CSCs); Endothelial progenitor cells (EPCs); Chronic ischemic injury; Strain imaging; Left ventricular remodeling

INTRODUCTION

Transplantation of somatic tissue-derived stem cells has been shown to be a feasible, safe, and potentially effective treatment for advanced cardiac failure in clinical settings (6,32). In particular, cardiac stem cells (CSCs), represented by c-kit-positive cells in the myocardium, can play a central role in healing the damaged myocardium, through their direct differentiation in situ, the recruitment of circulating stem/progenitor cells, or the paracrine release of cardioprotective factors (9,12,30). CSC transplantation is therefore considered a promising treatment for advanced cardiac failure, although the optimal method for cell delivery into the heart is still under debate (7).

The transplantation of scaffold-free cell sheets was shown to enhance the retention and survival of the transplanted cells and to minimize the risks of cell delivery-related myocardial damage that leads to arrhythmogenicity, thus showing good therapeutic potential (5,20,33). However,

Received July 26, 2012; final acceptance March 17, 2013. Online prepub date: April 3, 2013.
Address correspondence to Professor Yoshiki Sawa, Department of Cardiovascular Surgery, Osaka University Graduate School of Medicine, 2-2 Yamadaoka, Suita, Osaka 565-0871, Japan. Tel: +81-6-6879-3154; Fax: +81-6-6879-3163; E-mail: sawa-p@surg1.med.osaka-u.ac.jp

concerns remain regarding the integration of the transplanted cells into the myocardium, which would have a direct impact on regional cardiac function, and the potential for ischemia in the transplanted cell sheet, which would limit its therapeutic potential. On the other hand, endothelial progenitor cells (EPCs) have been shown to induce neoangiogenesis in the ischemic/infarcted myocardium and to activate residential CSCs to enhance healing and/or regeneration of the damaged myocardium (11,13,31). The intramyocardial injection of EPCs is thus another promising treatment for enhancing myocardial regeneration and possibly supporting the cellular function of transplanted CSCs (16).

We thus hypothesized that CSC transplantation by the cell sheet technique might induce cardiomyogenic differentiation in situ, reverse left ventricular (LV) remodeling, and improve functional recovery in ischemic injury model and that these therapeutic effects might be enhanced by the concomitant transplantation of EPCs, which could have different effects on the damaged myocardium from CSCs.

Several lines of evidence suggested that region-specific, especially layer-specific, LV function assessed by recently developing modalities may be superior to globally measured ejection fraction (EF) in predicting myocardial recovery after a wide range of medical and surgical treatment (3,14). Here we used a porcine chronic ischemic injury model to dissect the layer-specific functional effects of these two types of cell transplantation.

MATERIALS AND METHODS

All human and animal studies were carried out with the approval of the institutional ethical committee. Human samples were collected under written informed consent. The investigation conforms to the Principles of Laboratory Animal Care formulated by the National Society for Medical Research and the NIH guidelines for the care and use of laboratory animals. All experimental procedures and evaluations were carried out in a blinded manner.

Isolation and Cultivation of C-Kit-Positive Cells From Human Cardiac Tissue

Human normal right atrial tissues were obtained from a 53-year-old female patient with dilated cardiomyopathy at Osaka University Hospital. The isolation method was as published recently (6). Briefly, after dissecting fat and fibrous tissue, the sample was cut into small pieces (<1 mm^3) and suspended in 8 ml Ham's F12 medium (Wako Pure Chemical Inc., Osaka, Japan) containing 0.2% collagenase (17454; Serva Electrophoresis, Heidelberg, Germany). After digestion, cells were plated in culture dishes (353003; BD Falcon, Franklin Lakes, NJ, USA) containing Ham's F12 supplemented with 10% fetal bovine serum (FBS; SH30406.02; Hyclone, Thermo Scientific, Waltham, MA, USA), 10 ng/ml recombinant human basic fibrobrast growth factor (bFGF; 100-18B; PeproTech, Rocky Hill, NJ, USA), 0.2 mM L-glutathione (G6013; Sigma-Aldrich, St. Louis, MO, USA), and 5 mU/ml erythropoietin (E5627-10UN; Sigma Aldrich). Subsequently, cells were expanded and subjected to fluorescence-activated cell sorting (FACSAria; BD Biosciences, San Jose, CA, USA) with antibody {cluster of differentiation 117-phycoerythrin [CD117(AC126)-PE]; also known as c-kit or stem cell growth factor receptor, 130-091-735; Miltenyi Biotec, Bergisch Gladbach, Germany} to obtain c-kit-positive CSCs. The sorted c-kit-positive CSCs were cultured until the fifth passage in the above medium (30).

Preparation of CSC Sheet and Endothelial Progenitor Cells

Cultured CSCs were characterized by fluorescence-activated cell sorting (FACS) analysis, labeled by 2 μM DiI-red (Molecular Probes, Eugene, OR, USA) (33), and then incubated on 10-cm thermoresponsive dishes (Cell Seed Inc., Tokyo, Japan) at 37°C for 12 h. The DiI-red-labeled CSCs spontaneously detached from the dish surface following incubation at 20°C for 30 min, yielding a CSC sheet. Each CSC sheet was approximately 42 mm in diameter and 100 μm thick. Granulocyte colony-stimulating factor-mobilized EPCs of human origin (AllCells, MPB-017F; Emeryville, CA, USA) were labeled with 2 μM DiI-blue in vitro (Molecular Probes) (33). The following monoclonal antibodies were used: c-kit allophycocyanin (APC) [A3C6E2 (clone), 130-091-733; MiltenyiBiotec], CD105 PE (FAB10971P; R&D Systems, Minneapolis, MN, USA), CD34 fluorescein isothiocyanate (FITC) (555821, BD Biosciences), CD31 PE (FAB3567P, R&D Systems), 7-aminoactinomycin D peridinin–chlorophyll protein–cyanine 5.5 [7AAD PerCP-Cy5-5; 51-68981E (559925); BD Biosciences], immunoglobulin G1(IgG1)–FITC isotype controls (555748; BD Biosciences), IgG1–APC isotype controls (130-092-214; Miltenyi Biotec), and IgG1–PE isotype controls (IC002P; R&D Systems).

Generation of the Swine Chronic Ischemic Injury Model and Cell Transplantation

A 2.5-mm ameroid constrictor (Tokyo Instruments, Inc., Tokyo, Japan) was placed around the proximal left anterior descending artery via a left thoracotomy in female swine (Clawn miniature, 1 year old, 25 kg; Japan Farm, Inc., Kagoshima, Japan). A total of 65 swines were then cared for in a temperature-controlled individual cage with a daily intake of 5 mg/kg cyclosporin A (Novartis, East Hanover, NJ, USA) (15). Multidetector CT identified 52 pigs that developed a left ventricular ejection fraction (LVEF) between 30% and 40% at 21 days post-ameroid placement. Since eight of these pigs died prior to cell transplantation, a total of 44 pigs were randomly divided

into four treatment groups ($n=11$ in each): sham operation (sham group), CSC sheet transplantation only (CSC-only group), intramyocardial injection of EPCs (EPC-only group), and CSC sheet transplantation plus EPC injection (CSC–EPC group). After a median sternotomy under general anesthesia, three-layered CSC sheet (total 1×10^8 cells) was placed on the epicardium of the ischemic area [left anterior descending (LAD) region] and stitched in place around the edge. EPCs (total 2.5×10^6 cells) were intramyocardially injected into 12 different sites of the ischemic and peri-ischemic area. After the transplantation and/or intramyocardial injection was completed, the pericardium was closed. The pigs were taken care of for 1 day ($n=1$ each), 3 weeks ($n=4$ each), or 8 weeks ($n=6$ each), when they were sacrificed in a humane manner.

Continuous Electrocardiogram Monitoring

The electrocardiogram (ECG) was monitored during 5 days posttreatment with the Holter system (Unique Medical Co., Tokyo, Japan) for swines sacrificed at 8 weeks after cell transplantation ($n=6$ each group). The heart rate and arrhythmia events during the first 24 h were analyzed using software (Softron Co., Tokyo, Japan).

Multidetector CT and Conductance Catheterization

Global LV function was assessed by multidetector computed tomography (CT) at pretreatment and 8 weeks posttreatment ($n=6$ each) and by cardiac catheterization at 8 weeks posttreatment ($n=5$ each). After infusing 45 ml of nonionic contrast agent (Iomeron 350; Eisai Co., Tokyo, Japan) via the ear vein, 5-mm slice images of the entire heart were obtained in the craniocaudal direction using a 16-slice CT scanner (Emotion 16; Siemens, Tokyo, Japan). Every 10% of the R-R interval was reconstructed to calculate the LVEF and end-diastolic/systolic volume (EDV and ESV, respectively) using software (Lexus, Aze Inc., Tokyo, Japan).

Pressure–volume (P-V) cardiac catheterization was performed after median sternotomy by inserting a conductance catheter (Unique Medical) and a microtip catheter transducer (SPR-671; Millar Instruments, Inc., Houston, TX, USA) into the LV cavity. The P-V loop data under stable hemodynamics or inferior vena cava occlusion were analyzed with Integral 3 software (Unique Medical).

Speckle-Tracking Echocardiography and Myocardial Contrast Echocardiography

Short-axis echocardiographic images, obtained using the Artida 4D Echocardiography System (Toshiba Medical Systems Co., Tochigi, Japan) and PST-30SBT transducer, were analyzed by the speckle-tracking method using wall motion-tracking software (Toshiba Medical Systems) (2,4). End-systolic radial strain (RS) values at the mid and apical levels were averaged in a layer-specific manner to measure the endocardial and epicardial wall motion index (WMI), respectively.

Myocardial contrast echocardiography was performed using real-time contrast pulse sequencing operating on the Aplio ultrasound system (Toshiba Medical Systems) (8). Briefly, after an intravenous injection of 20 ml of ultrasound contrast agent (Sonazoid, Daiichi Sankyo Inc., Parsippany, NJ, USA), images in the apical two-chamber view were acquired to score the myocardial opacification using Volmac software (YD Ltd., Nara, Japan).

Histology

Cultured CSCs on eight-well Lab-Tec chamber slides were fixed with 4% paraformaldehyde (163-20145, Wako Pure Chemical Inc.), labeled, and examined by confocal microscopy (FV300, Olympus, Tokyo, Japan). Alexa Fluor-488 phalloidin (Molecular Probes) was used to enhance the background actin filaments. Paraffin-embedded transverse sections at the papillary muscle level were stained with Masson's trichrome (MT; Masson's Trichrome staining kit, Muto Pure Chemicals, Tokyo, Japan), and the amount of interstitial collagen at the entire LV wall was semiquantified by MetaMorph software (Molecular Devices, Sunnyvale, CA, USA) ($n=6$, in each). In addition, the thickness of the ventricular wall was measured at two points from the LV posterior area and two points from the interventricular septum, and results were expressed as the average of the four points. Five-micrometer cryosections were subjected to either periodic acid-Schiff (PAS) staining (PAS staining kit, Muto Pure Chemicals) or immunohistolabeling. The following primary antibodies were used: rabbit anti-c-kit (1:50; Dako Co., Glostrup, Denmark), rabbit anti-von Willebrand factor (vWF; 1:500; Dako), mouse anti-Ki-67 (1:50; Dako), rabbit anti-connexin 43 (1:200; Sigma Aldrich), mouse anti-cardiac troponin I (cTn-I; 1:100; Abcam Co., Cambridge, UK), mouse anti-stromal cell-derived factor 1(SDF-1; 1:50; Abcam), rabbit anti-vascular endothelial growth factor (VEGF; 1:100; Thermo Scientific), and rabbit anti-insulin-like growth factor 1 (IGF-1; 1:100; Abcam). Capillary density was expressed as the average number of vWF-positive circular structures in five randomly selected sections, corrected for the total area of the tissue section measured. PAS-stained sections were used to determine the cell diameter of the cardiomyocytes at the remote zone. DiI-red-positive cells were traced by MetaMorph software to quantify the area of engrafted clusters of CSC sheet.

Reverse Transcription Polymerase Chain Reaction (RT-PCR)

Total RNA was extracted from the CSCs and the swine heart tissues posttreatment using an RNeasy Kit (Qiagen, Hilden, Germany), then reverse-transcribed using Omniscript Reverse Transcriptase (Qiagen) and

amplified using the Gene Amp® PCR System 9700 (Life Technologies, Tokyo, Japan). The primer pairs were as follows: human-specific kinase insert domain receptor (KDR or VEGF receptor 2) primer sequence, sense CCT CTA CTC CAG TAA ACC TGA TTG GG, antisense TGT TCC CAG CAT TTC ACA CTA TGG; human-specific chemokine C-X-C motif receptor 4 [CXCR4 or stromal-derived factor 1 (SDF-1) receptor] primer sequence, sense ACG TCA GTG AGG CAG ATG, antisense GAT GAC TGT GGT CTT GAG; human glyceraldehyde-3-phosphate dehydrogenase (GAPDH) primer sequence, sense AAT GGG CAG CCG TTA GGA AA, antisense GCG CCC AAT ACG ACC AAA TC; swine-specific SDF-1 primer sequence, sense CCGAACTGTGCCCTTCAGAT, antisense ATAA ACATCCCGCCGTCCTC; swine-specific CXCR-4 primer sequence, sense GCGCAAAGCTCTCAAAACCA, antisense CAGTGGAAAAAGGCAAGGGC; swine-specific VEGF primer sequence, sense GAC GTC TAC CAG CGC AGC TAC T, antisense TTT GAT CCG CAT AAT CTG CAT G; swine-specific IGF-1 primer sequence, sense ACA TCC TCT TCG CAT CTC TTC TAC TT, antisense CCA GCT CAG CCC CAC AGA; swine GAPDH primer sequence, sense CTG CAC CAC CAA CTG CTT AGC, antisense GCC ATG CCA GTG AGC TTC C. The transcript level of GAPDH was used as an endogenous reference. The products from the cultured CSCs were stained with ethidium bromide (Bio-Rad Laboratories, Hercules, CA, USA), separated by electrophoresis (Mupid submarine electrophoresis system, Advance Co. Ltd., Tokyo, Japan) on an agarose gel (Agarose S, Nippon Gene Co., Ltd., Tokyo, Japan), and quantified.

Fluorescence In Situ Hybridization (FISH)

Paraffin-embedded sections were predenatured, dehydrated, and then labeled with deoxyribonucleic acid probes, a Cy3-conjugated probe for human-specific genome, Cy5-conjugated probe for swine-specific genome (Chromosome Science Laboratory, Hokkaido, Japan), and mouse anti-cTn-I or rabbit anti-vWF. The sections were visualized with secondary antibodies conjugated to Alexa fluorochromes. Nuclei were labeled with 4,6-diamino-2-phenylindole (DAPI; Molecular Probes).

Statistical Analysis

Continuous data are summarized as medians with ranges (minimums to maximums) or means ± SEM (standard error of mean) and are plotted in figures with raw values or barplots of the means with symmetric SEM bars, as appropriate. Distributions of the continuous data were checked for normality with the Shapiro–Wilk test and for equality of between-group variances with the Levene test. Normally distributed data were compared between four groups using the analysis of variance (ANOVA), followed by the Tukey multiple comparison for equal variances, or Welch's ANOVA, followed by the Games–Howell multiple comparison for unequal variances. Nonnormally distributed data were compared using the Kruskal–Wallis test, followed by the Steel–Dwass multiple comparison. Normally and nonnormally distributed data before and after treatment were compared using the paired t test and the Wilcoxon signed rank-sum test, respectively. All p values are two-sided, and values of $p<0.05$ were considered to indicate statistical significance. All analyses were performed with the SPSS 11.0J for Windows (SPSS, Chicago, IL, USA) and the R program (http://www.r-project.org/) (10).

RESULTS

Human Atrium-Derived C-Kit-Positive Cells Showed CSC Characteristics In Vitro

The isolated right atrium-derived cells were characterized in vitro by FACS, immunohistolabeling, and RT-PCR analyses. The proportion of c-kit-positive cells at the second passage was 99±4% (Fig. 1A and B). However, as the cells expanded, they lost the primitive phenotype, and more than half of them had the potential to differentiate to the endothelial rather than the cardiomyocyte or smooth muscle cell lineage. The proportion of c-kit-positive cells at the fifth passage was 20±10%, while 34%, 71%, and 99% of them expressed CD34, CD31, and CD105, respectively (Fig. 1C). Immunohistochemistry revealed that approximately 5% of the cells expressed cTn-I in the cytoplasm (Fig. 1D). In addition, RT-PCR clearly revealed the expression of CXCR4 and KDR in the cells (Fig. 1E).

After incubating the cells on temperature-responsive dishes at 37°C for 12 h, CSC sheets were generated by lowering the temperature. Each cell sheet was approximately 42 mm in diameter, and the gap junction protein connexin 43 was expressed between the cells (Fig. 1F). Most of the cells expressed the proliferation marker Ki-67 in their nucleus (Fig. 1G).

Successful Cell Transplantation With Minimal Arrhythmogenicity

A total of 44 pigs underwent treatment, which was performed without any procedure-related mortalities ($n=11$ each). Fatal arrhythmias, such as ventricular tachycardia and fibrillation, or composite ventricular arrhythmias (grades 3–5 in Lown's classification) were not detected in any group during the first 24 h posttreatment, as assessed by Holter ECG monitoring ($n=6$ each) (Table 1). There were no significant differences in the heart rate or number of unifocal premature ventricular/atrial contractions among the groups.

Global Functional Recovery After CSC Sheet Transplantation Was Enhanced by EPC Injection

Multidetector CT measured LVESV, LVEDV, and LVEF, and cardiac catheterization measured the systolic

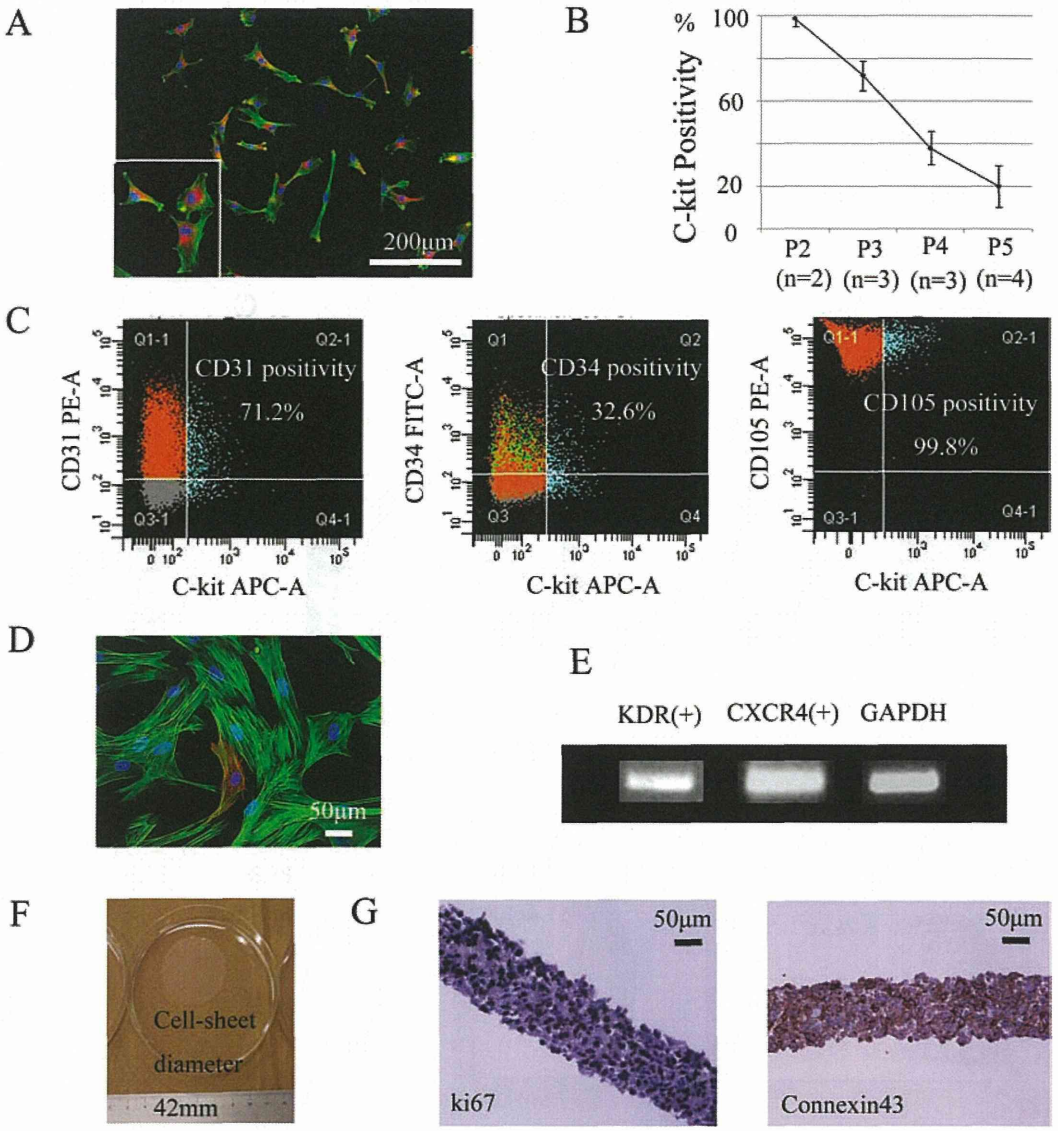

Figure 1. Characterization of the CSC sheet in vitro. (A) Representative double immunostaining for c-kit (red) and phalloidin (green) of cultured CSCs at the second passage. (B) C-Kit positivity was markedly decreased by passage culture. (C) FACS analysis of cultured CSCs at the fifth passage. (D) Cultured CSCs at the fifth passage expressed myocyte structural protein, a characteristic of cardiac progenitor cells. Phalloidin (green), troponin I (red). (E) RT-PCR analysis of CSCs at the fifth passage. (F) Detached CSC sheet. (G) Representative immunostaining for Ki-67 or connexin 43. Nuclear staining by DAPI is shown in blue in (A) and (D). Abbreviations: CSC, cardiac stem cell; FACS, fluorescence-activated cell sorting; CD31, cluster of differentiation 31; RT-PCR, reverse transcription polymerase chain reaction; KDR, kinase insert domain receptor; CXCR4, chemokine C-X-C motif receptor 4; GAPDH, glyceraldehyde 3-phosphate dehydrogenase; DAPI, 4,6-diamino-2-phenylindole.

Table 1. Evaluation of Fatal Arrhythmia by 24-h ECG Monitoring Posttransplantation

	Heart Rate (bpm)				PVC				
Group	Max Beat	Min Beat	Mean Beat	PAC	Singlet	Couplet	Triplet	VT	Vf
Sham ($n=6$)	181±42	83 (52–118)	102 (62–137)	208 (126–297)	35 (6–65)	0	0	0	0
EPC-only ($n=6$)	189±31	100 (53–132)	113 (71–163)	254 (102–377)	55 (21–83)	0	0	0	0
CSC-only ($n=6$)	171±29	55 (50–79)	97 (45–101)	120 (44–201)	19 (9–58)	0	0	0	0
CSC–EPC ($n=6$)	172±17	83 (42–92)	101 (48–169)	250 (145–377)	48 (15–77)	0	0	0	0

Abbreviations: ECG, electrocardiogram; PAC, premature atrial contraction; PVC, premature ventricular contraction; VT, ventricular tachycardia; Vf, ventricular fibrillation; EPC, endothelial progenitor cell; CSC, cardiac stem cell.

parameters d*P*/d*t* max, end-systolic pressure–volume relation (ESPVR), and diastolic parameters: τ, end-diastolic pressure (EDP), and d*P*/d*t* min. There were no significant differences in LVESV, LVEDV, or LVEF among the group pretreatment (Fig. 2A–C). The pigs treated with the sham operation developed increases in LVESV ($p<0.001$) and LVEDV ($p<0.001$) but not in LVEF (34±5% to 32±6%, $p=0.44$) in 8 weeks. In contrast, the pigs in the EPC-only or CSC-only group showed preserved LVESV (EPC-only, $p=0.23$; CSC-only, $p=0.89$), LVEDV (EPC-only, $p=0.15$; CSC-only, $p=0.13$), and LVEF (EPC-only, 37±5% to 37±4%, $p=0.91$; CSC-only, 36±4% to 43±5%, $p=0.12$). Moreover, the combined treatment induced a significant decrease in LVESV ($p=0.04$) and a significant increase in

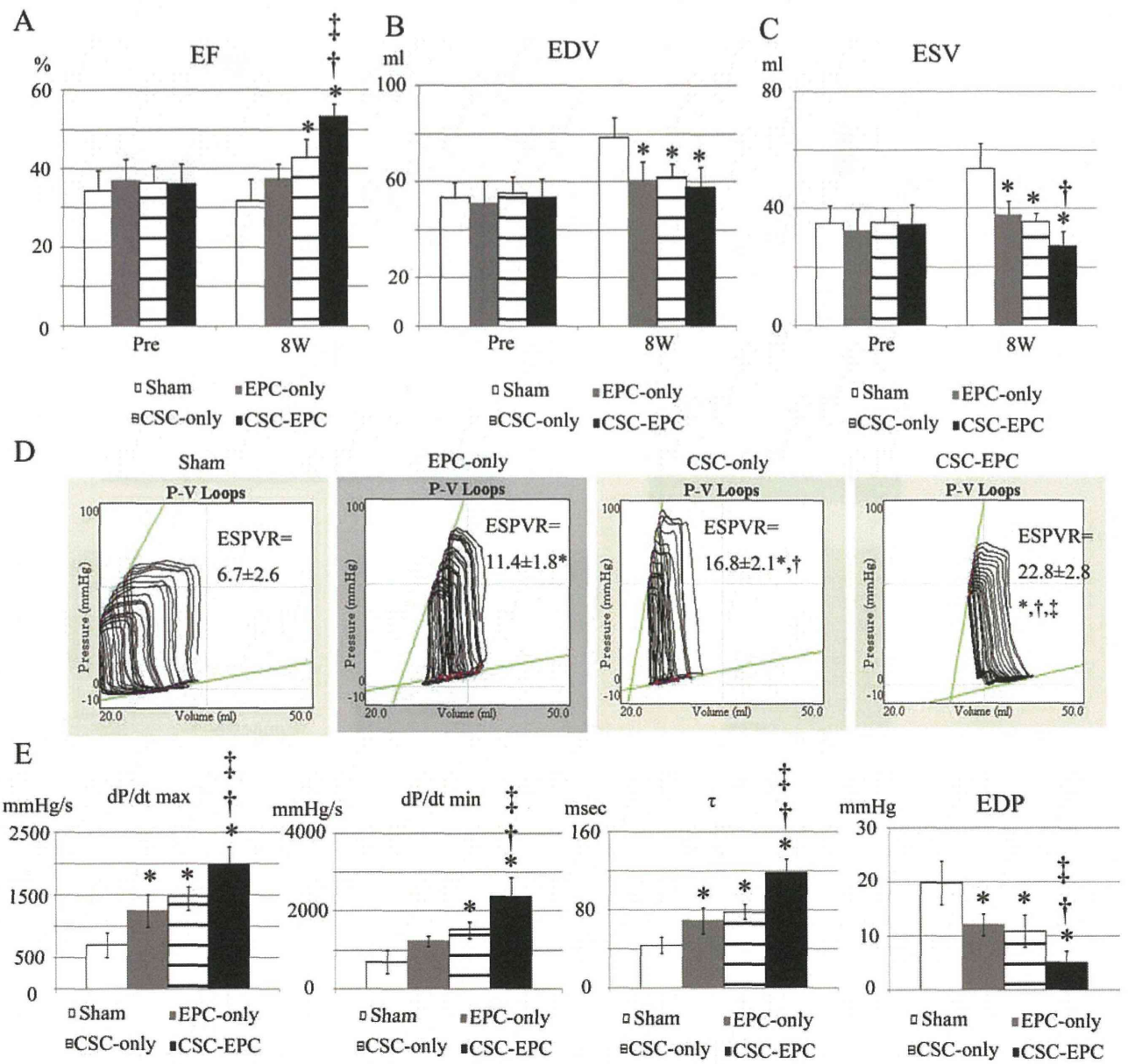

Figure 2. Global LV function assessed by multidetector CT and conductance catheter. (A–C) Multidetector CT parameters [(A) EF, (B) EDV, (C) ESV] before and 8 weeks after cell transplantation ($n=6$ each). (D) Representative P-V loops during IVC occlusion for each group at 8 weeks posttreatment ($n=5$ each). ESPVR of the CSC–EPC group was the greatest followed by that of the CSC-only group, then the EPC-only group, and then the sham group ($p<0.001$, ANOVA). (E) d*P*/d*t* max, d*P*/d*t* min, τ and EDP ($n=5$ each). *$p<0.05$ versus sham, †$p<0.05$ versus EPC-only, ‡$p<0.05$ versus CSC-only. Abbreviations: LV, left ventricle;CT, computed tomography; EF, ejection fraction; EDV, end-diastolic volume; ESV, end-systolic volume; P-V, pressure-volume; IVC, inferior vena cava; ESPVR, end-systolic pressure-volume relationship; CSC, cardiac stem cell; EPC, endothelial progenitor cell; EDP, end-diastolic pressure.

LVEF (36±5% to 53±3%, $p=0.001$) in the 8 weeks following cell transplantation.

At 8 weeks posttreatment, the LVESV of the CSC-only and EPC-only groups was significantly smaller than that of the sham group, and the LVESV of the CSC–EPC group was even smaller than that of the EPC-only group ($p<0.001$ for CSC–EPC, CSC-only, and EPC-only vs. sham, and for CSC–EPC vs. EPC-only). The LVEDV of the CSC–EPC, CSC-only, and EPC-only groups was significantly smaller than that of the sham group ($p=0.001$ for CSC–EPC, CSC-only, and EPC-only vs. sham). The LVEF of the CSC-only group was significantly greater than that of the sham group, while the LVEF of the CSC–EPC group was even greater than that of the other groups ($p<0.001$ for CSC-EPC vs. CSC-only, EPC-only, and sham, and for CSC-only vs. sham). Moreover, the ESPVR of the CSC–EPC group was the greatest, followed by that of the CSC-only group, then the EPC-only group, and then the sham group (Fig. 2D).

The dP/dt max, τ, EDP, and absolute value of dP/dt min were significantly greater in the CSC–EPC group than in the CSC-only and EPC-only groups, and these values except for the absolute value of dP/dt min were significantly greater in the CSC-only and EPC-only groups than in the sham group (Fig. 2E).

Differential Region- or Layer-Specific Effects by CSC and EPC Transplantation

Region- or layer-specific systolic LV function was assessed using speckle-tracking echocardiography, which was carried out at pretreatment and at 4 and 8 weeks posttreatment ($n=6$). There was no significant difference in the endocardial or epicardial wall motion index in the ischemic anterior area among the groups at pretreatment (Fig. 3A and B).

The pigs given the sham operation developed a significant decrease in the epicardial wall motion index (10±2% to 7±1%, $p=0.01$) and no change in the endocardial wall motion index (10±1% to 9±1%, $p=0.40$) in 8 weeks. In contrast, cell transplantation induced a significant increase in epicardial [CSC-only, 10±2% to 18 (14–28)%, $p=0.03$; CSC–EPC, 10±1% to 20±5%, $p=0.01$] and endocardial (EPC-only, 10±1% to 12±1%, $p=0.01$; CSC–EPC, 10±1% to 14±1%, $p=0.001$) indices at 8 weeks.

At 8 weeks posttreatment, the epicardial wall motion index of the CSC–EPC and CSC-only groups was significantly greater than that of the EPC-only or sham group ($p<0.001$ for CSC–EPC and CSC-only vs. EPC-only and sham) (Fig. 3A and C). In contrast, the endocardial wall motion index of the CSC–EPC group was the greatest followed by that of the EPC-only group, and both were significantly greater than that of the CSC-only or sham group ($p<0.001$ for CSC–EPC vs. EPC-only vs. CSC-only and sham) (Fig. 3B and D).

Consistent with these findings, the myocardial perfusion score in the ischemic zone at 8 weeks posttreatment was significantly greater in the CSC–EPC (36±1 dB) than in the sham group (19±2 dB, $p<0.001$) (Fig. 3E and F).

Engraftment of Transplanted CSCs and EPCs and Neovascularization of the Infarcted Wall

The engraftment of transplanted DiI-red-labeled CSCs and DiI-blue-labeled EPCs was examined, and the capillary density was assessed by fluorescence-based immunohistolabeling for vWF. At 3 weeks after cell transplantation, most of the transplanted CSCs were present over the ischemic area in the sheet shape, although no DiI-red- or DiI-blue-positive cells could be seen in any heart slice at 8 weeks posttreatment (Fig. 4A and B). The number of vWF-positive capillaries in the ischemic epicardium of the CSC–EPC and CSC-only groups was significantly greater than in the EPC-only or sham group (CSC–EPC, 251±84/mm^2; CSC-only, 257±43/mm^2; EPC-only, 105±20/mm^2; sham, 112±23/mm^2; $p=0.001$ for CSC–EPC and CSC-only vs. EPC-only and sham) (Fig. 4C). In contrast, the number of capillaries in the ischemic endocardium was significantly greatest in the CSC–EPC, followed by the EPC-only group, and then by the CSC-only or sham group (CSC–EPC, 269±11/mm^2; EPC-only, 193±14/mm^2; CSC-only, 108±30/mm^2; sham, 74±38/mm^2; $p<0.001$ for CSC–EPC vs. EPC-only vs. CSC-only and sham). In association with these findings, some of the transplanted CSCs in both the CSC–EPC and CSC-only groups were observed in native epicardial tissues, while some had migrated into the endocardial tissues only in the CSC–EPC group (Fig. 4D). On the other hand, transplanted EPCs in both the CSC–EPC and EPC groups were observed in the ischemic and peri-ischemic area of the endocardium, especially near the vascular wall.

To elucidate the possible mechanism for the transplanted CSC migration, RT-PCR and immunostaining for angiogenic growth factors were performed ($n=4$ each). The mRNA levels of swine-specific SDF-1, VEGF, and IGF-1 were upregulated in all the treatment groups (Fig. 5A). In particular, the mRNA levels of SDF-1 and the SDF-1 receptor CXCR4 were markedly greater in the CSC–EPC group than in the other groups (SDF-1 or CXCR4: $p<0.001$ for CSC–EPC vs. CSC-only, EPC-only, and sham). In addition, SDF-1, but not VEGF or IGF-1, was expressed in the cytoplasm of the transplanted CSCs that were present in the native myocardial tissue in the CSC–EPC group (Fig. 5B).

Preserved Myocardial Integrity 8 Weeks After Cell Transplantation

Interstitial fibrosis and capillary density in the heart at 8 weeks posttreatment were assessed by MT (Fig. 6A) and PAS (Fig. 6B) staining and immunohistolabeling for vWF (Fig. 6C), respectively ($n=6$ each). Excluding

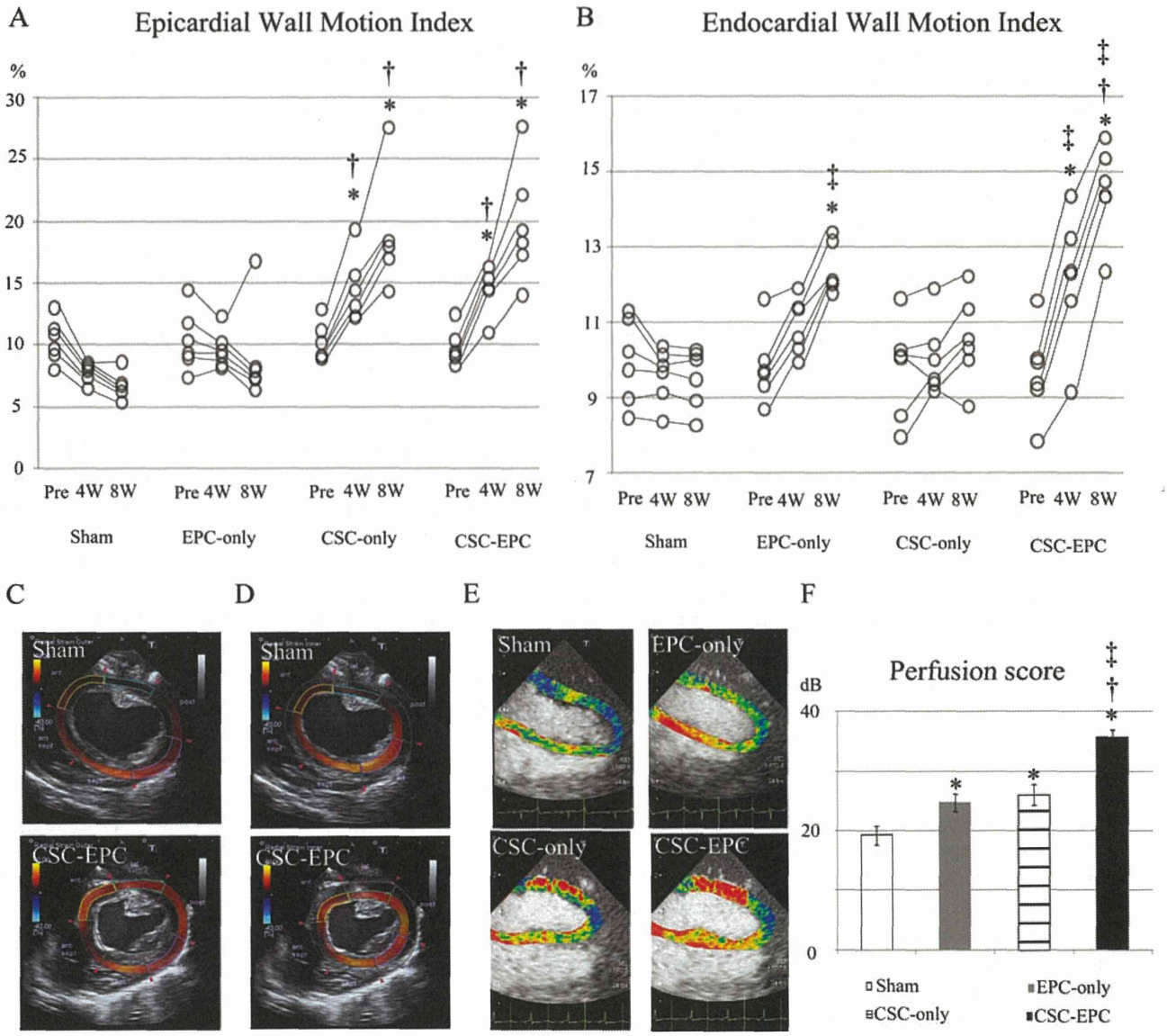

Figure 3. Region- and layer-specific systolic LV function and myocardial perfusion assessed by speckle-tracking and real-time contrast echocardiography. (A, B) Epicardial (A) and endocardial (B) WMIs in the ischemic area before, 4 and 8 weeks after cell transplantation ($n=6$ each). At 8 weeks posttreatment, the epicardial WMI of the CSC–EPC and CSC-only groups was significantly greater than that of the EPC-only or sham group ($p=0.001$, Kruskal–Wallis test), while the endocardial WMI of the CSC–EPC group was the greatest followed by that of the EPC-only group, and then the CSC-only and sham group ($p<0.001$, ANOVA). (C, D) Representative epicardial (C) and endocardial (D) radial strain images at end-systole in the CSC–EPC and sham groups. (E) Representative contrast echocardiography 2D-imaging visualized by Volmac software in each group. (F) Myocardial perfusion scores 8 weeks posttreatment ($n=6$). Myocardial perfusion score in the ischemic zone was significantly greater in the CSC–EPC than in the sham group ($p<0.001$, ANOVA) *$p<0.05$ versus sham, †$p<0.05$ versus EPC-only, ‡$p<0.05$ versus CSC-only. Abbreviations: LV, left ventricular; 2D, two-dimensional; CSC, cardiac stem cell; EPC, endothelial progenitor cell; WMI, wall motion index.

the sham group, there were no significant differences in infarct area among the other groups. On the other hand, the accumulation of collagen or area of chronic ischemic injury was the smallest in the CSC–EPC group followed by the CSC-only and EPC-only groups, and then by the sham group (CSC–EPC, 7 ± 1%; CSC-only, 15 ± 3%; EPC-only, 20 ± 3%; sham 28 ± 5%; $p<0.001$ for CSC–EPC vs. CSC-only and EPC-only vs. sham) (Fig. 6D). The LV wall thickness was significantly larger in the CSC–EPC group than in the sham group (CSC–EPC, 9 ± 1 mm; sham 7 ± 1 mm; $p<0.01$ for CSC–EPC vs. sham) (Fig. 6E).

The myocyte cell diameter at 8 weeks posttreatment was assessed in the 5-mm heart sections of the remote zone stained by PAS ($n=6$ each). The myocyte diameter

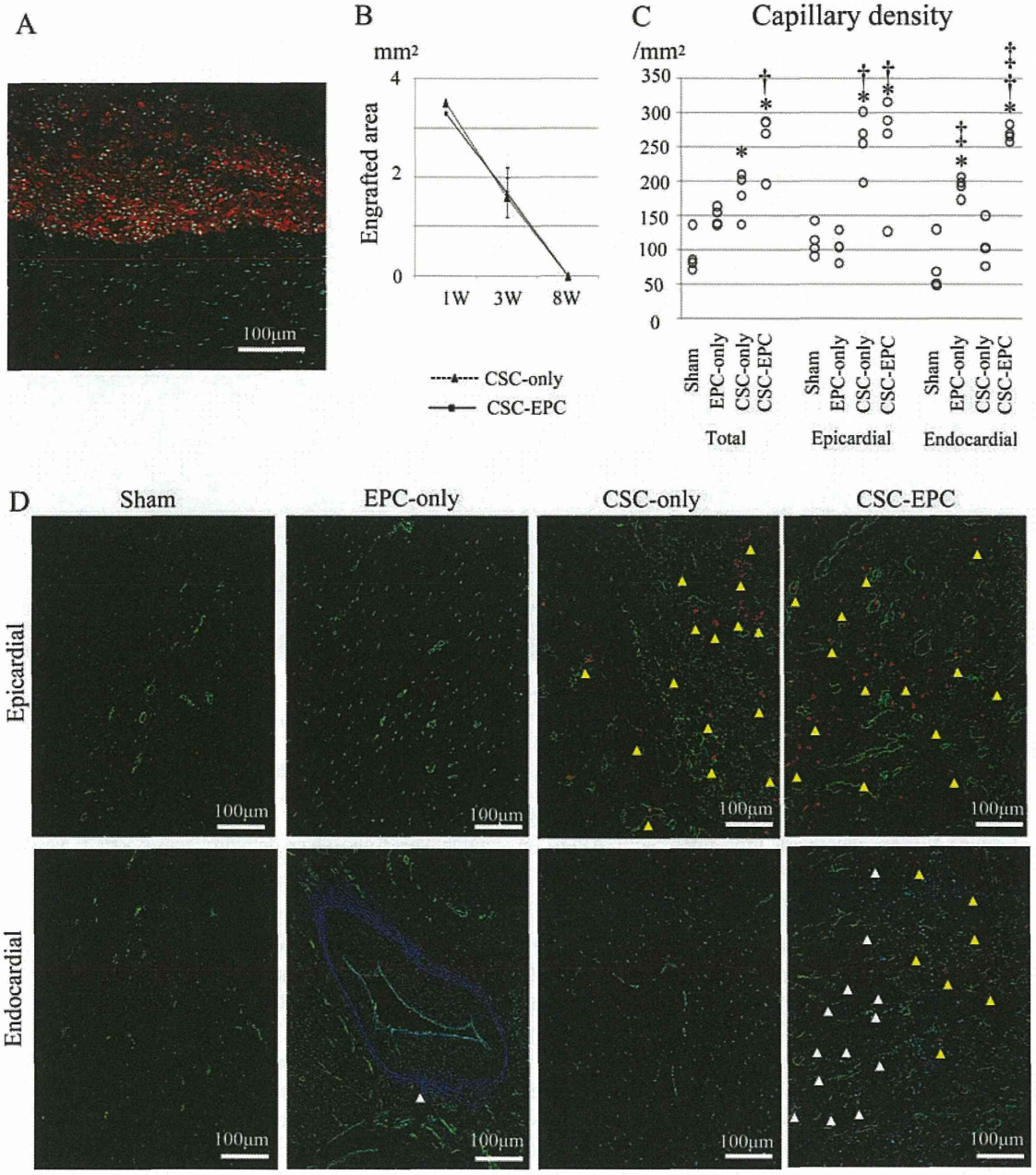

Figure 4. Engraftment of transplanted CSCs and EPCs and neovascularization of the ischemic wall. (A) Engraftment of the transplanted DiI-red-labeled CSC sheets (red) at 3 weeks posttreatment. (B) Quantification of the CSC sheet engrafted area in the CSC-only and CSC–EPC groups 1, 3, and 8 weeks posttreatment. (C) Quantification of the vWF-positive capillary density at the ischemic epicardium and endocardium in each group at 3 weeks posttreatment. The number of vWF-positive capillaries in the ischemic epicardium of the CSC–EPC and CSC-only groups was significantly greater than in the EPC-only or sham group ($p<0.001$, ANOVA), while the number of capillaries in the ischemic endocardium was significantly greatest in the CSC–EPC, followed by the EPC-only group, and then by the CSC-only and sham groups ($p<0.001$, ANOVA). (D) Representative immunostaining for vWF (green) at the ischemic epicardium and endocardium at 3 weeks posttreatment in each group. Migration of CSCs into the ischemic endocardium was observed only in the CSC–EPC group, and not in the CSC-only group. Yellow and white arrows indicate CSCs and EPCs, respectively. *$p<0.05$ versus sham, †$p<0.05$ versus EPC-only, ‡$p<0.05$ versus CSC-only. Nuclear staining by DAPI is shown in blue in (A) and (D). Abbreviations: CSC, cardiac stem cell; vWF, von Willebrand factor.

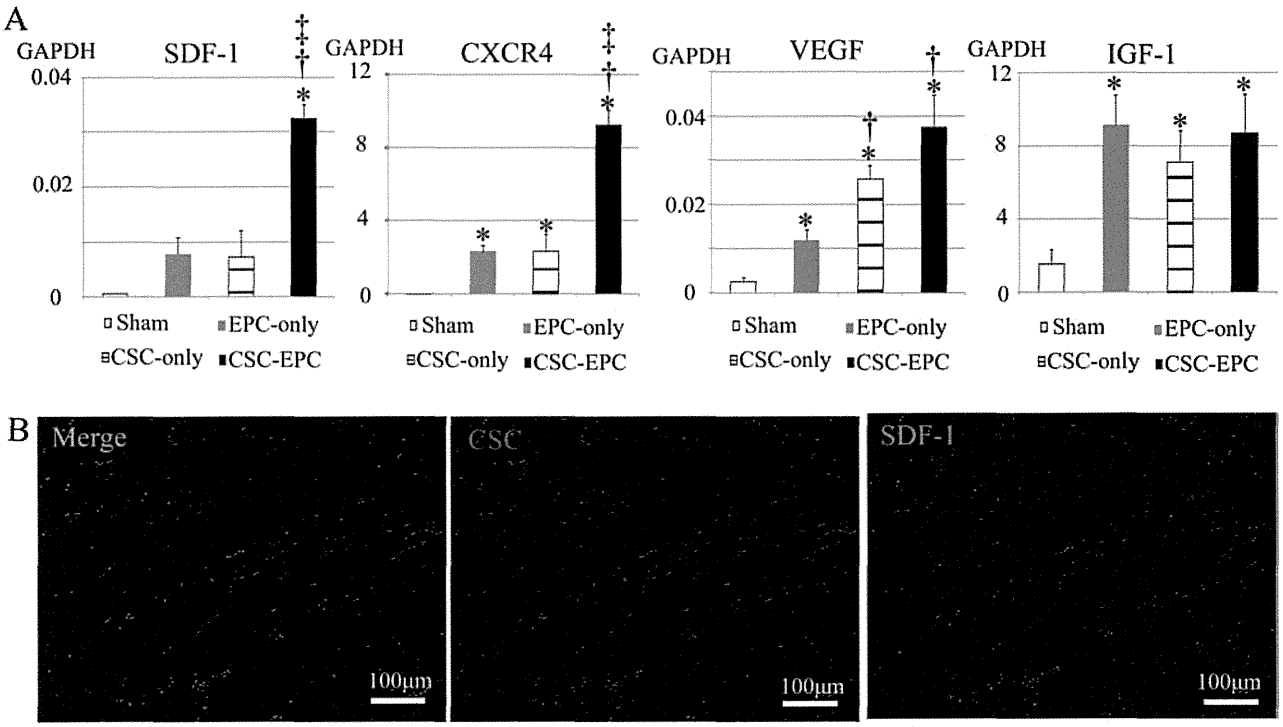

Figure 5. Possible mechanism of CSC migration. (A) RT-PCR analysis in each group at 3 weeks posttreatment. The mRNA levels of swine-specific SDF-1 ($p<0.001$, Welch's ANOVA) and CXCR4 ($p<0.001$, Welch's ANOVA) were markedly greater in the CSC–EPC group than in the other groups ($n=4$ each). (B) Representative immunostaining for SDF-1 in the CSC–EPC group at 3 weeks posttreatment. DiI-red-labeled CSCs (middle panel), SDF-1 (green) (right panel), and merged image (left panel). Nuclear staining by DAPI is shown in blue. *$p<0.05$ versus sham, †$p<0.05$ versus EPC-only, ‡$p<0.05$ versus CSC-only. Abbreviations: CSC, cardiac stem cell; RT-PCR, reverse transcription polymerase chain reaction; SDF-1, stromal cell-derived factor 1; CXCR4, chemokine C-X-C motif receptor type 4; EPC, endothelial progenitor cell; GAPDH, glyceraldehyde 3-phosphate dehydrogenase; VEGF, vascular endothelial growth factor; IGF-1, insulin-like growth factor-1.

was significantly smaller in the CSC–EPC group than in the CSC-only, the EPC-only, or the sham group (CSC–EPC, 33±9 mm; CSC-only, 49±10 mm; EPC-only, 55±8 mm; sham 61±8 mm; $p<0.001$ for CSC–EPC vs. CSC-only, EPC-only, and sham) (Fig. 6F).

The number of vWF-positive capillaries in the peri-ischemic zone of the CSC-only or EPC-only group was greater than that of the sham group, and the number of the CSC–EPC group was even greater than that of the EPC-only or sham group. (CSC–EPC, 83±11/mm^2; CSC-only, 74±6/mm^2; EPC-only, 62±8/mm^2; sham 32±10/mm^2; $p<0.001$ for CSC-only and EPC-only vs. sham, and for CSC–EPC vs. EPC-only and sham) (Fig. 6G). In addition, greater vessel formation with vascular lumen was induced in the CSC–EPC group compared with the other groups.

Phenotypic Fate of Transplanted CSCs and EPCs Posttransplantation

The phenotype of the transplanted CSCs and EPCs in the native myocardium at 8 weeks posttransplantation was histologically assessed by human- and/or swine-specific genome-based FISH analysis. Small numbers of cardiomyocytes and endothelial cells with a human genome in the nucleus were present in the native myocardium of both the CSC–EPC and CSC-only groups, but not in the EPC-only group (Fig. 7A and B). However, there was no difference in the number of cells with a human genome between the CSC–EPC and CSC-only groups. Of note, all the cells with a human genome in the nucleus also carried a swine genome in the nucleus and thus had chimeric nuclei (Fig. 7C and D).

DISCUSSION

We here demonstrated that primary c-kit-positive CSCs were successfully isolated from the human right atrium and expanded and showed that they had a differentiation potential for endothelial rather than cardiomyogenic lineages, in vitro. Human CSC sheets were successfully transplanted into the swine chronic ischemic injury heart with minimal arrhythmogenicity and elicited global functional recovery in 8 weeks. CSC sheet transplantation concomitant with intramyocardial EPC injection showed enhanced global functional recovery compared with the CSC sheet-only therapy. Transplantation of the CSC

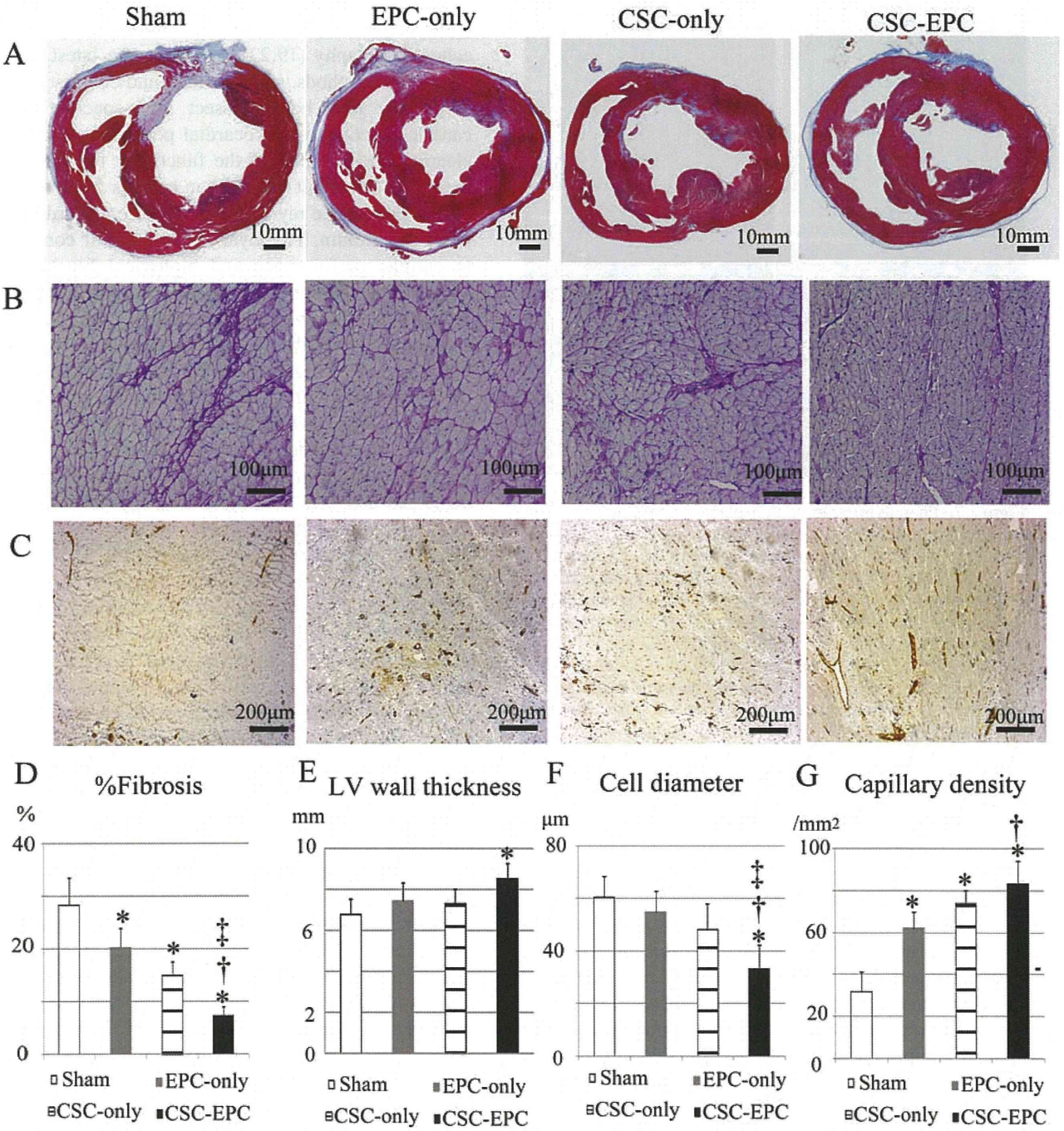

Figure 6. Histological assessment of interstitial fibrosis, capillary density, and myocyte hypertrophy 8 weeks after cell transplantation. (A) Representative Masson's trichrome staining in a section through the entire heart. (B) Representative periodic acid-Schiff staining of the remote zone. (C) Representative immunostaining for vWF in the peri-ischemic zone. (D) Quantification of fibrosis in each group ($n=6$ each). (E) In the CSC–EPC group, the thickness of the LV wall was well preserved compared with the sham group ($p<0.01$, ANOVA). (F) Quantification of the cell diameter of myocytes ($n=6$ each). (G) Quantification of capillary density at the peri-ischemic zone ($n=6$ each). The number of vWF-positive capillaries of the CSC–EPC group was the greatest, followed by the CSC-only and EPC-only groups, and then the sham group ($p<0.001$, ANOVA). *$p<0.05$ versus sham, †$p<0.05$ versus EPC-only, ‡$p<0.05$ versus CSC-only. Abbreviations: vWF, von Willebrand factor; CSC, cardiac stem cell; EPC, endothelial progenitor cell; LV, left ventricular.

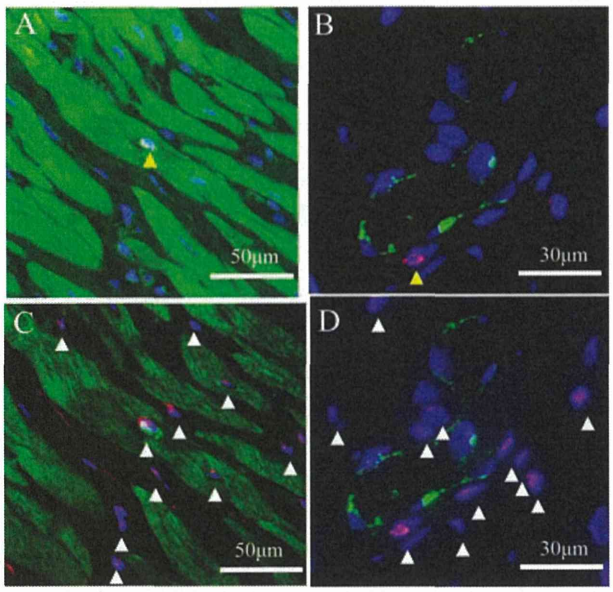

Figure 7. Phenotypic fate of transplanted CSCs and EPCs at 8 weeks posttreatment. (A, B) Representative immunostaining with human FISH (white/pink staining) and cTn-I (A; green) or vWF (B; green) in the CSC–EPC group. Small numbers of cardiomyocytes (A) and endothelial cells (B) with a human genome were present in the native myocardium. (C, D) Representative immunostaining with swine FISH and cTn-I (C) or vWF(D) in the CSC–EPC group. All the cardiomyocytes (C) and endothelial cells (D) that were positive for human genomic markers were also positive for porcine markers; thus, they had chimeric nuclei. Nuclear staining by DAPI is shown in blue. Yellow and white arrows indicate human and swine genomic markers, respectively. Abbreviations: CSC, cardiac stem cell; EPC, endothelial progenitor cell; FISH, fluorescence in situ hybridization; cTn-I, cardiac troponin I; vWF, von Willebrand factor.

sheet alone induced histological reverse LV remodeling, including attenuated interstitial fibrosis and increased vessel numbers, and concomitant EPC injection induced greater reverse LV remodeling effects than the CSC sheet-only therapy. Most of the transplanted CSCs were engrafted onto the surface over the ischemic area, while a small number migrated into the epicardium following the transplantation of the CSC sheet only. In contrast, concomitant EPC injection enhanced the migration of the transplanted CSCs into the myocardium, in association with local upregulations of SDF-1, VEGF, and IGF-1. While the CSCs of human origin in this study rarely differentiated into the cardiomyocytes in a porcine heart, transplantation of the CSCs induced functional and pathological recovery, suggesting that paracrine effects are the major therapeutic mechanisms in this study. Importantly, speckle-tracking echocardiography and histological data indicate that the CSCs and the EPCs produced different paracrine effects in the failing heart, suggesting synergic effects of these two cell types as shown in this study.

Clinical cell therapy has been reported to yield only modest functional recovery, as assessed by standard echocardiography (19,22). However, the latest echocardiographic methods, such as strain and contrast echocardiography, may better dissect layer-specific regional cardiac functions or myocardial perfusion, leading to a clearer understanding of the functional benefits of cell therapies. The adult mammalian heart is formed in three layers: contractile myocardium, inner endocardium, and outer epicardium. The layers differ in their contribution to cardiac performance and biological function (18). Myocardial infarction affects these myocardial layers to different extents, and ischemic change occurs in a wavefront pattern from the endocardium to the epicardium. In particular, the epicardium is thought to have a rich cardiac progenitor cell niche and to play an important role in cardiac repair (18,24,34). Of note, it has been shown that cell sheet implantation into the epicardium induces the expression of multiple cardioprotective factors in the heart and activates host epicardial cells crucial for cardiac repair through "crosstalk" between the implanted cell sheet and the native epicardium (20,33). This delivery method has also been demonstrated to maximize the retention and survival of the transplanted cells and to minimize the risks of cell delivery-related myocardial damage (23,27). Thus, we believed that the transplantation of CSCs by the cell sheet technique might have greater therapeutic effects in a swine chronic ischemic injury model than other delivery methods.

Our layer-specific analysis by strain echocardiography revealed that the CSC sheet transplantation induced significant functional improvement in myocardial function only in the ischemic epicardium. Consistent with this result, epicardial CSC sheet implantation induced neovascularization and reduced fibrosis in a paracrine manner in this area. We also observed the migration of transplanted CSCs into the native ischemic epicardium, which suggested that these functional and morphological benefits might be associated with the location of transplanted CSCs in the host myocardium. Previous reports demonstrated that the SDF-1–CXCR4 axis plays an important role in the migration of bone marrow and cardiac stem cells from the cell sheet to the infarct myocardium (17,28,29). Our data suggested that since migrated CSCs were located in the vicinity of SDF-1 in the host tissue, SDF-1 present in the ischemic tissue might promote the cell migration from the cell sheet to the native ischemic tissues. The strong expression of CXCR4 in the CSC sheet in vitro might support this scenario. In fact, the expressions of angiogenic growth factors, including SDF-1, in the chronic ischemic tissues were markedly diminished in the sham group, although these cytokines and adhesion molecules, which play important roles in cardiac repair after injury, are known to be abundant in